Lozano-Cruz, T. et al. (2020) 'Cationic Carbosilane Dendritic Systems as Promising Anti-Amyloid Agents in Type 2 Diabetes', Chemistry : a European journal, 26(34), pp. 7609–7621.

Available at https://doi.org/10.1002/chem.202000091

Manuscript submitted to *Chemistry – A European Journal*

Article Type*: Regular Article.*

Corresponding Author: Paula Ortega López

Department of Organic and Inorganic Chemistry

University of Alcalá

UAH Campus. Faculty of Pharmacy

28871 Alcalá de Henares. Spain.

Tel: (+34) 91 8854679. Fax: (+34) 91 8854683.

E-mail: paula.ortega@uah.es

CATIONIC CARBOSILANE DENDRITC SYSTEMS AS PROMISING ANTI-AMYLOID AGENTS IN TYPE 2 DIABETES

Tania Lozano-Cruz,[1,2,3] Gema Alcarraz-Vizán,[4,5] F. Javier de la Mata,[1,2,3] Sara de Pablo,[4] Paula Ortega,[1,2,3]∗ Yorley Duarte,[6] Felipe Bravo-Moraga,[6] Fernando D. González-Nilo,[6,7] Anna Novials[4,5], Rafael Gómez. [1,2,3]∗

[1]Department of Organic and Inorganic Chemistry, and Research Institute in Chemistry "Andrés M. Del Río" (IQAR), University of Alcalá, Madrid, Spain.

[2]Networking Research Center on Bioengineering, Biomaterials and Nanomedicine (CIBER-BBN), Spain. E-mail: paula.ortega@uah.es.

[3] Ramón y Cajal Health Research Institute (IRYCIS), IRYCIS, Spain.

[4]Diabetes and Obesity Research Laboratory, Institut d'Investigacions Biomédiques August Pi i Sunyer (IDIBAPS), Hospital Clínic de Barcelona, Barcelona, Spain;

[5]Spanish Biomedical Research Centre Diabetes and Associated Metabolic Disorders (CIBERDEM) (CIBERDEM), Spain

[6]Center for Bioinformatics and Integrative Biology, Faculty of Life Science, Universidad Andres Bello University, Santiago, Chile

[7]Interdisciplinary Center for Neuroscience of Valparaíso, Faculty of Science, University of Valparaíso, Valparaíso, Chile

KEYWORDS

Dendrimers, dendron, chaperone, IAPP, diabetes

ABSTRACT

The most common denominator of many of the neurodegenerative diseases is the badly folded protein accumulation resulting in the formation of insoluble protein deposits located in different parts of the organism, causing cell death and tissue degeneration. Dendritic systems have turned out to be a promising new therapeutic approach for the treatment of these diseases due to their ability to modulate the folding of these proteins. In this perspective, and focused on Type 2 Diabetes (T2D) characterized by the presence of deposits containing amyloidogenic islet amyloid polypeptide (IAPP), we present how different topologies of cationic carbosilane dendrimers inhibit the deposit formation in pancreatic islets isolated from Tg-hIAPP mice. Also, the results obtained by the modification of dendritic carbosilane wedges with a chemical chaperone, 4-phenyl butyric acid (4-PBA), at the focal point confirmed their promising potential as anti-amyloid agents with a concentration efficiency five order of magnitude lower than that observed for the free 4-PBA in the therapeutic action. Computational studies, that determine at the atomic level the main interaction between IAPP and dendrimers, supported the experimental work.

INTRODUCTION

Notwithstanding the rigorous cellular mechanisms of regulation and assistance to protein folding, there are numerous examples of badly folded protein accumulation, which self-assemble and associate forming aggregates or deposits in different parts of the organism, causing cell death and tissue degeneration. Although the primary sequences of the peptides and proteins that form these deposits, called amyloid deposits, are different, all of them are characterized by presenting a secondary structure in the form of a β-sheet which gives them the property of insolubility leading to the formation of oligomers and fibrils. Despite the fact that different pathological proteins are associated to each disease, it is possible that the pathology of all of them occurs by means of common mechanisms that are related to the formation of similar amyloid inclusions.[1] During the last two decades, at least 40 diseases have been recognized in which the aggregation of different proteins is involved in the so called amyloid diseases. Some of these are rare, like primary amyloidosis or amyloid light-chain (AL) amyloidosis,[2] while others are very common, such as Alzheimer's disease (amyloid β peptide, Aβ),[3] Parkinson's disease or Lewy body dementia (alpha-synuclein, AS),[4] amyotrophic lateral sclerosis (superoxide dismutase, SOD),[5] Huntington's disease (polyglutins, Poli-Q),[6] spongiform

encephalopathies (prion protein, Prp),[7] frontotemporal dementias (aggregation of tau or ubiquitin),[8] or Type 2 Diabetes (T2D) (islet amyloid polypeptide, IAPP).[9]

Type 2 Diabetes (T2D)[10] is a common and chronic disease characterized among others by an impaired insulin secretory capacity and a decline in β-cell mass and function. The mechanism by which T2D diabetes progresses is unclear, but it is suggested that one of the factors involved in the evolution of the disease is related to misfolding of islet amyloid polypeptide (IAPP). IAPP is normally co-localized and co-secreted together with insulin and contributes to the maintenance of glucose homeostasis. Its accumulation may lead to the establishment of toxic protein aggregates and, eventually, endoplasmic reticulum (ER) stress and cell death.[9a, 11]

Even though there are several drugs used to palliate and/or prevent the formation of protein aggregates, these disorders are chronic and there are currently no effective treatments to avoid their progression, using palliative and symptomatic methods to face the course of the disease. Among them the so-called chemical chaperones, that are a kind of low molecular weight compounds, could stabilize the conformation of proteins against thermal stress as well as inhibit the formation of badly folded structures and therefore prevent the formation of amyloid fibers.[12] One example of a chemical chaperone is 4-phenyl butyric acid (4-PBA), which can act by reversing the processes of anomalous localization and/or protein aggregation associated with certain human diseases.[13]. Some studies have demonstrated that PBA treatment in mice overexpressing the amyloidogenic human IAPP (hIAPP) in pancreatic β cells prevents and reverses pancreatic islet amyloid formation in hIAPP transgenic islets cultured at high glucose concentrations.[14]

The interaction between nanotechnology and medicine is an opportunity to carry out new treatments or improve existing ones, to be driven the design and use of nanoscopic systems as drug delivery or as anti-amyloid agents *per se*.[15] In this sense, dendrimers or dendritic systems, due to their unique properties, such as their monodisperse structure and high multifunctionalization capacity, have turned out to be ideal systems to increase the solubility and lifetime in circulation of diverse drugs or bioactive molecules, since they cross certain tissues, improving the passageway through biological barriers.[16] There are several dendritic systems of different topologies such as PAMAM,[17] glycodendrimer,[18] phosphorus[19] and carbosilane[20] that are being studied in the treatment of diseases associated with protein accumulation and shown to be effective in preventing the bad folding of proteins. For example, low generation anionic dendrimers or OH-terminated PAMAM dendrimers have the capacity to modulate the self-assembly of IAPP, accelerating or preventing the accumulation.[21] Also, cationic poly(propyleneimine) dendrimers functionalized with maltose reduce amyloid cytotoxicity on PC12 and SH-SY5Y cells.[22] Also, low generation sulphated dendrimers have been shown to be effective in the prevention of protein accumulation, interfering in the

mechanic of the IAPP fibrillation and inhibit its proteotoxicity, by accelerating amyloid formation or by capturing the peptide in a non-aggregating and non-toxic shape.[23]

Herein, we presented the capacity of cationic carbosilane dendritic system to prevent the formation of IAPP deposits and the way that dendrimer topology determine their effect on aggregation. In addition, from this information, dendritic wedges of different generation functionalized with the chaperone fragment 4-phenyl butyric acid (4-PBA) at the focal point were prepared in order to evaluate the anti-amyloid combination effect of both moieties in T2D. Finally, the molecular behaviour and estimated binding free energy of each dendrimer-IAPP complex were studied to evaluate the structural impact on IAPP through MD simulations and MD/GBSA calculation respectively.

RESULTS AND DISCUSSION

Selection of dendritic topology

In this study, the prevention of amyloid islet deposition in mice overexpressing hIAPP in pancreatic islets under the influence of carbosilane dendritic systems of different topologies was determined. For it, $G_1Si(SNMe_3I)_8$ (**I**) as spherical dendrimer, $HOC_6H_4OG_3(SNMe_3I)_8$ (**II**) as a dendron (both previously synthesized elsewhere in our research group)[24] and the here-prepared bow-tie system $(IMe_3NS)_4G_2[OC_6H_4O]G_2(SNMe_3I)_4$ (**3**) (see **Figure 2** for representative structures) were selected. These systems present in their structure the same number of ammonium groups per molecule.

First of all, in order to assess the influence of topology, it was necessary to synthesize a bow-tie dendritic system. Hydroquinone molecule was chosen as core since both the location of the hydroxyl groups in the *para* position and the rigidity of the aromatic ring allow the distribution of the dendritic carbosilane wedges without suffering a high steric impediment. The carbosilane dendron chosen (**IV**) presents a bromide atom at the focal point as good leaving group that can react easily with the hydroxyl groups by nucleophilic substitution, while the vinyl moieties on the surface can be subsequently functionalized with ammonium groups by thiol-en coupling reaction with 2-dimethyl-aminoethanethiol hydrochloride (see **Scheme 1**). The synthetic protocol used was the same as that described elsewhere for obtaining spherical carbosilane cationic dendrimers derived from $1,3,5\text{-}C_6H_3(OH)_3$.[25] The bow-tie $[(IMe_3NS)_4G_2](OC_6H_4O)[G_2(S\text{-}NMe_3I)_4]$ (**3**) was obtained as white solid in good yields and this compound as well as its precursors **1** and **2** were characterized through NMR spectroscopy and ESI-TOF (see section 2: Methods).

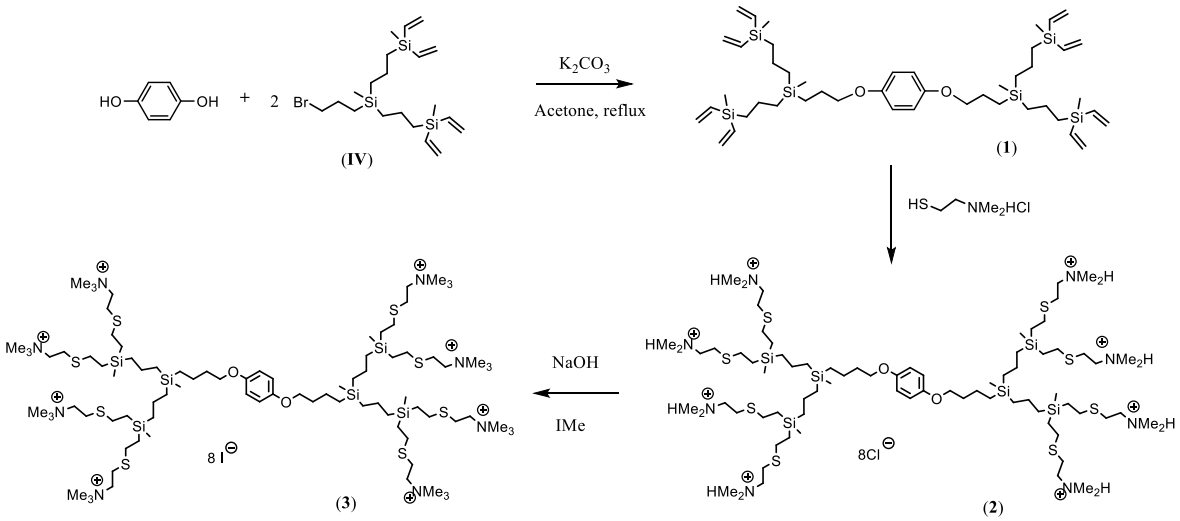

Scheme 1. Synthetic protocol for bow-tie dendrimer **3** and its precursors.

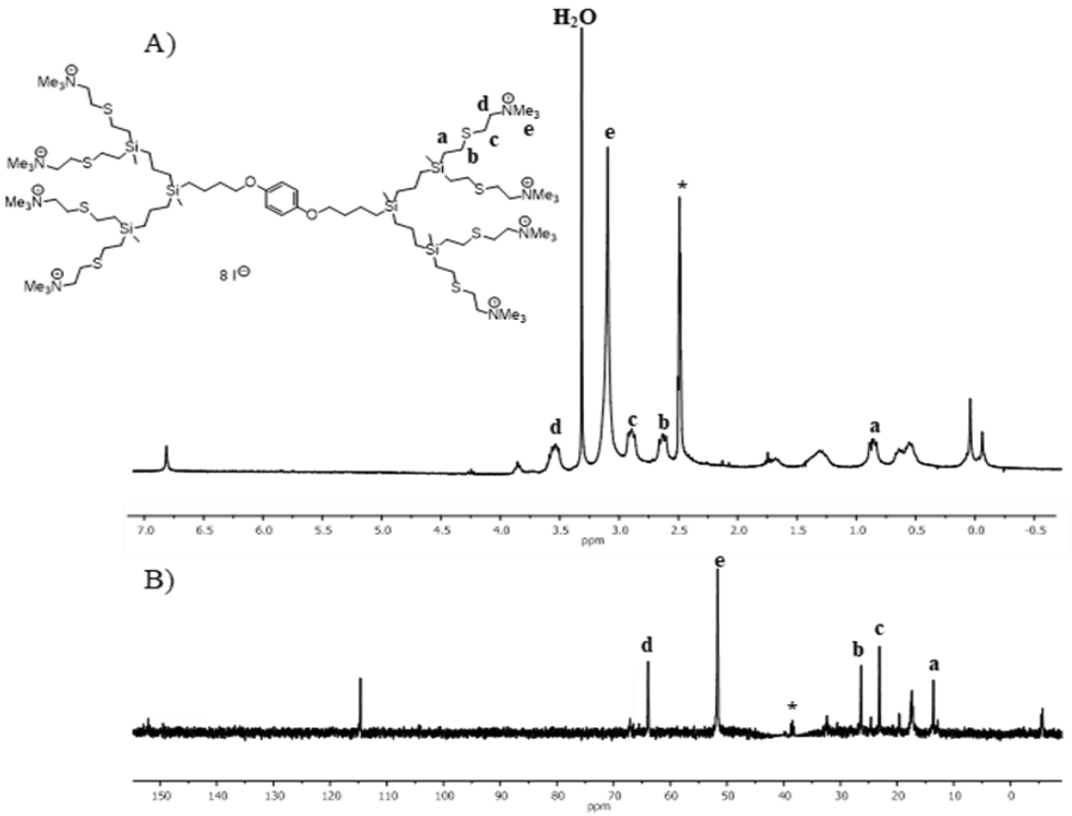

Figure. 1. ^{1}H NMR- (A) y ^{13}C-NMR-{^{1}H} (B) of $(IMe_3NS)_4G_2[OC_6H_4O]G_2(SNMe_3I)_4$ **(3)** . *****DMSO-d_6

Presence and severity of amyloid in pancreatic islets treated with dendritic systems.

To begin evaluating the anti-amyloidogenic capacity of dendritic systems we carried out the studies in isolated islet from transgenic mice (Tg-mice). Despite the fact that Tg-hIAPP mice exhibit a glucose intolerance phenotype, amyloid deposits cannot be detected until the animals reach an advanced age and are fed a high-fat diet. However, function and survival of β-cells are markedly affected when Tg-hIAPP islets are cultured under high glucose conditions generating amyloid deposits.[26] To carry out the first trial of the anti-amyloidogenic activity of dendritic compounds, pancreatic islets from 10-12 weeks old Tg-hIAPP mice extracted by perfusion with collagenase and gradient with Histopaque, were treated with a single dose of 5μM of each compound ($G_1Si(SNMe_3I)_8$ (**I,** spherical), $HOC_6H_4OG_3(SNMe_3I)_8$ (**II,** dendritic wedge) and $(IMe_3NS)_4G_2[OC_6H_4O]G_2(SNMe_3I)_4$ (**3,** bow-tie). All of them present the same positive charges on the structure. The pancreatic islets were cultured together with the dendritic compounds for 7 days under high glucose conditions (HG= 16.7 mM). In these conditions, the isolated pancreatic islets from mice that overexpress the hIAPP generate amyloid deposits. Once the 7 days of culture were elapsed, the viability of pancreatic islets was analysed by microscopic loupe counting in relation to the initial number of islets at the beginning of treatment. Next, the inhibition of amyloid formation was measured by confocal laser scanning microscopy. The results obtained by two independent experiments revealed that bow-tie dendrimer **3** and the dendritic wedge **II** prevented amyloid formation by significant reduction of amyloid severity. Surprisingly, the spherical dendrimer **I** did not affect the severity of amyloid at all (see **Figure 2**). The dendron structure seems to be the adequate topology for obtaining greater interactions with IAPP while the spherical system did not interact probably because this topology is bulky enough to prevent such interactions. In the case of the bow-tie structure, the moderate activity is consistent with the interaction of one of the two dendritic wedges of the molecule imposed by the rigid hydroquinone core.

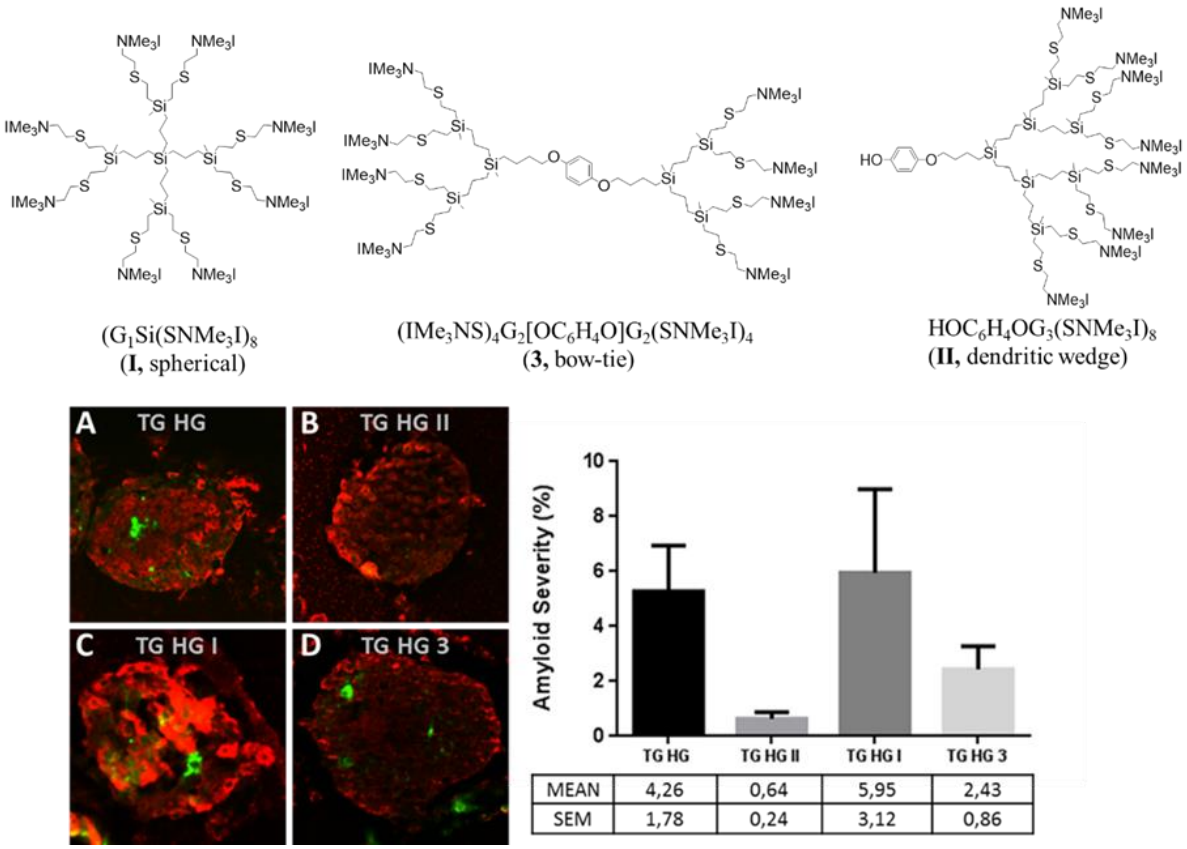

$(G_1Si(SNMe_3I)_8$
(I, spherical)

$(IMe_3NS)_4G_2[OC_6H_4O]G_2(SNMe_3I)_4$
(3, bow-tie)

$HOC_6H_4OG_3(SNMe_3I)_8$
(II, dendritic wedge)

Figure. 2. hIAPP Tg islets in high glucose conditions (HG, 16.7 mM glucose) during 7 days: A) untreated, B) treated with dendron **II**, C) treated with spherical dendrimer **I**, D) treated with bow-tie **3**. Amyloid was determined by fluorescence; in red, insulin (pancreatic islet immunohistochemistry) and in green, thioflavin (amyloid staining). Right panel, quantification of amyloid severity with the different compounds.

Molecular modelling was performed to understand at the atomistic level the main interaction between IAPP and dendrimers. IAPP is 37-amino acid residue peptide hormone of sequence KCNTATCATQRLANFLVHSSNN***FGAIL***SSTNVGSNTY containing a disulphide bridge between residues 2 and 7. With the exception of 1-7 region of IAPP, the entire length of this polypeptide has shown amyloidogenic properties at some stages, being region 23-27 the most prevalent one as folding area (see bold letters in the sequence). This fragment, FGAIL, forms β-sheet-containing fibrils that coil around each other in typical amyloid fibril morphology.[27]

The molecular simulation study conducted for spherical dendrimer **I** showed a strong interaction with the terminal residues 30-36 and the free energies involved in dendrimer-peptide binding were estimated by combining MD simulation and molecular mechanics/generalized Born surface area (MMGBSA) with a value of -7.7 Kcal/mol for spherical-IAPP complex. However, during MD simulation weak interaction was observed in the inner most 23-27 amyloidogenic region (see **Figure 3**), explaining molecularly the absence of anti-amyloidogenic activity. Such as spectrum of interaction is consistent with a bulkier structure self-imposed by the spherical

architecture. Respecting the bow-tie dendrimer **3**, weak interaction on the 30-36 residues and even weaker for the amyloidogenic region FGAIL were observed, with a total peptide-binding time less than 50% during the simulation, and free energy value of -7.4 Kcal/mol. These results are a consequence of the rigid structure offered by the hydroquinone core spreading all its structure and therefore the peripheral positive charges all over the peptide. The presence of only half of the positive charges and the carbosilane skeleton near to the amyloidogenic Asn22, Phe23, Ala25, Ile26, and Leu27 residues may explain the moderate activity shown respecting to the dendron system **II**. Finally, the notable hydrophobic and electrostatic interactions between dendron **II** and the terminal residues Thr30, Asn31, Val32, Asn35 and Tyr37 during ~45% of the simulation, could contribute with a free energy value of -8.0 Kcal/mol which may be the responsible of the high anti-amyloid activity observed for this topology. Without doubt, this shape can accommodate more efficiently a greater number of charges nearby the amyloidogenic region than the bow-tie shape.

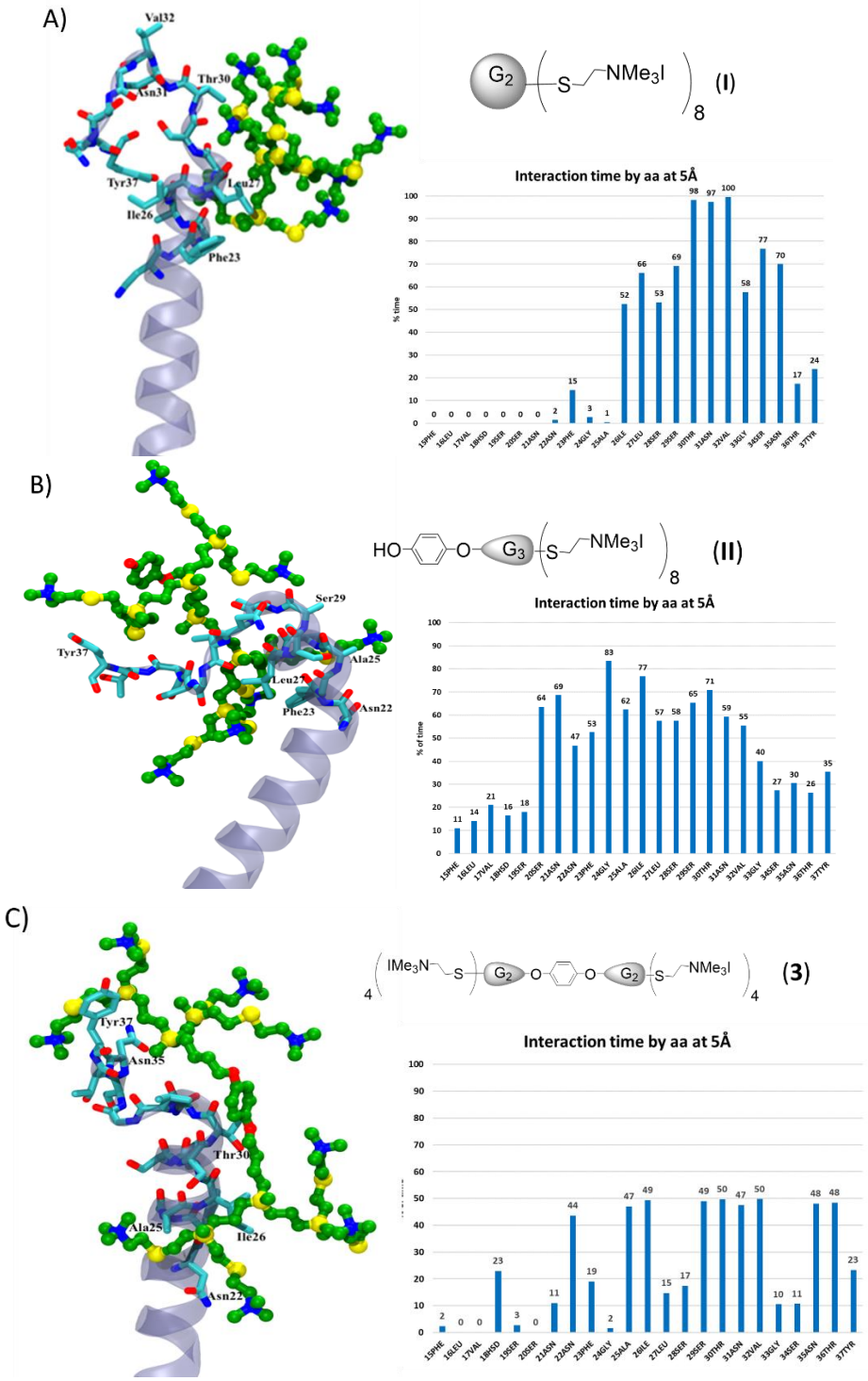

Figure 3. Molecular modelling of carbosilane dendritic systems of different topologies and the analysis of the interaction with IAPP peptide A) spherical (**I**), (B) dendron (**II**), (C) bow-tie (**3**).

Synthesis and chemical behavior of dendronized chaperones

Based on the preliminary experimental data and corroborated by molecular modelling studies, spherical and bow-tie topology were excluded for the subsequent experiments due to their low,

moderate or lack of anti-amyloidogenic activity. In order to improve the benefits observed for the dendron topology, it is interesting to obtain therapeutic systems that combine two active agents in the same structure through the capabilities that the dendron-shaped scaffold provides.

As mentioned before, the use of chemical chaperones in the treatment of diseases in which amyloid accumulations are involved, has become a hopeful therapeutic strategy. In these sense, 4-PBA is a chemical chaperone that could facilitate the correct folding of nascent proteins, such as hIAPP. The covalent combination of both fragments may promote synergisms between the two different therapeutic agents.[14, 20] For this purpose, a systematic strategy has been designed that allows the functionalization of carbosilane wedges with 4-PBA at the focal point and ammonium groups at the surface since both have shown to be interesting anti-amyloid agents.

Also, the election of two dendritic wedges with different focal point, hydroquinone (fron dendron **II**) and 4-PBA, to study their anti-amyloid capacity, will allow to establish if there is a synergistic effect between fragments with anti-amyloid activity (4-PBA and cationic charges of the dendritic surface).

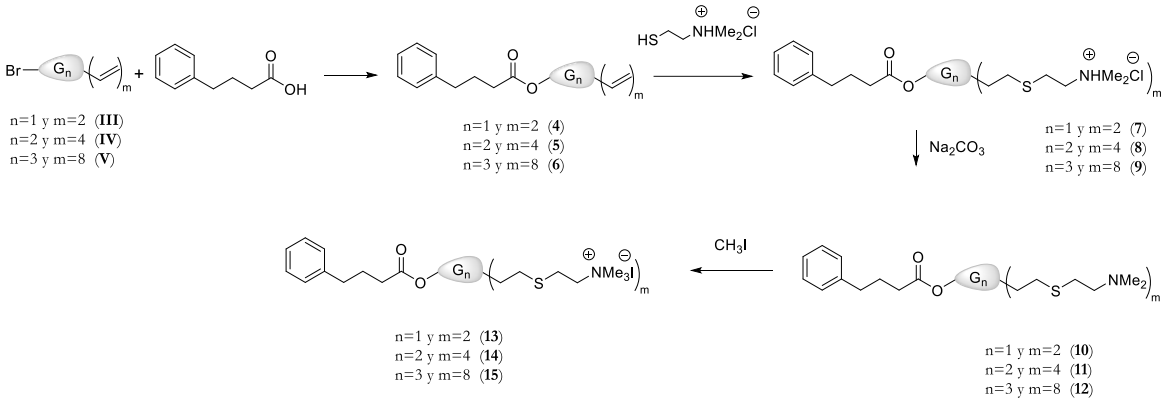

Scheme 2. Synthetic protocol for the preparation of ammonium-terminated carbosilane dendron containing 4-PBA at the focal point.

The attachment of 4-PBA to the dendritic system has been carried out by esterification reaction between the carboxylic acid moiety of 4-PBA and the bromide atom located at the focal point in dendrons of type BrG_nV_m previously described.[28] Thereby, the compounds $ArCO_2G_nV_m$ (n=1; m=2 (**4**), n=2; m=4 (**5**) y. n=3; m=8 (**6**)) were obtained as yellow oils. NMR spectroscopy confirmed the formation of the newly ester bond -$COOCH_2$- where the methylene group bonded to the focal point was located at 4.05 and 64.0 ppm in the ^1H and ^{13}C-NMR respectively. In addition, the ^{13}C-NMR spectra showed a signal corresponding to the carbonyl group at 173.5 ppm for ester group and the disappearance of the signal at 178.0 ppm attributed to the COOH in the free 4-PBA. Finally, thiol-ene coupling reaction with 2-dimethyl-aminoethanethiol hydrochloride, subsequent neutralization with $NaCO_3$ and quaternization with MeI (see Supporting Information) afforded the appropriate functionalization of the dendritic periphery

(see **Scheme 2**). Quaternization of amino groups with MeI was confirmed by displacement to low field of signals close to the nitrogen atom in the ^{1}H NMR spectrum respecting the neutral precursors. The cationic dendritic wedges $ArCO_2G_n(SNMe_3I)_m$ (n=1; m=2 (**13**), n=2; m=4 (**14**) and n=3; m=8 (**15**)) were obtained as yellow solids in excellent yields, soluble in water.

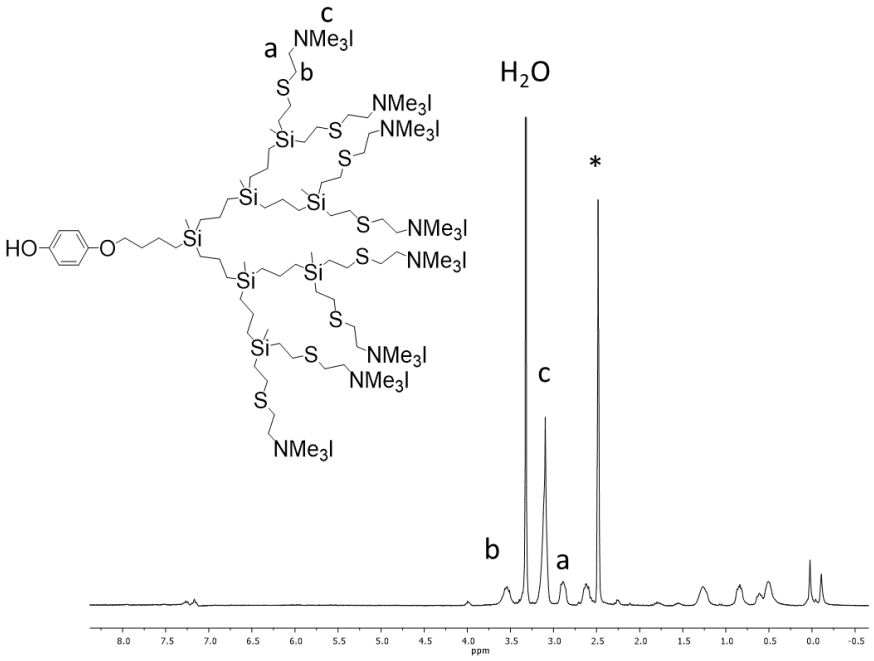

Figure 4. ^{1}H-NMR of $ArCO_2G_3(SNMe_3I)_8$ (**15**) in *****DMSO-d_6.

Knowing that the ester bond that binds 4-phenylbutyric acid to the dendritic skeleton could be degraded by various types of enzymes present in the organism, its stability was evaluated by HPLC when the compounds **13-15** were treated with pig liver esterase. The results showed the presence of free 4-PBA in all dendrons, although the release rate was clearly influenced by the dendritic generation. Thus, at 10 minutes of esterase addition, the percentage of free 4-PBA was approximately 37%, 18% and 3% for one (**13**), second (**14**) and third generation (**15**) respectively. After 7 days of incubation, it is possible to obtain the complete release for **13**, 70% for **14**, and only 20% of release for **15** even after a new addition of esterase, (see **Figure 5**). This behaviour is consistent with the results previously obtained in our research group for dendritic systems of similar topology with ibuprofen at the focal point linked by the same type of bond.[28] It is evidenced that by increasing the size of the dendritic skeleton, the group located at the focal point is less exposed and therefore the accessibility of esterase to the ester bond is compromised. This result indicates that the chaperone fragment is covalently sustained within the dendritic structure of dendron **15**, evidencing the existence of a single therapeutic entity with two different modes of anti-amyloid action.

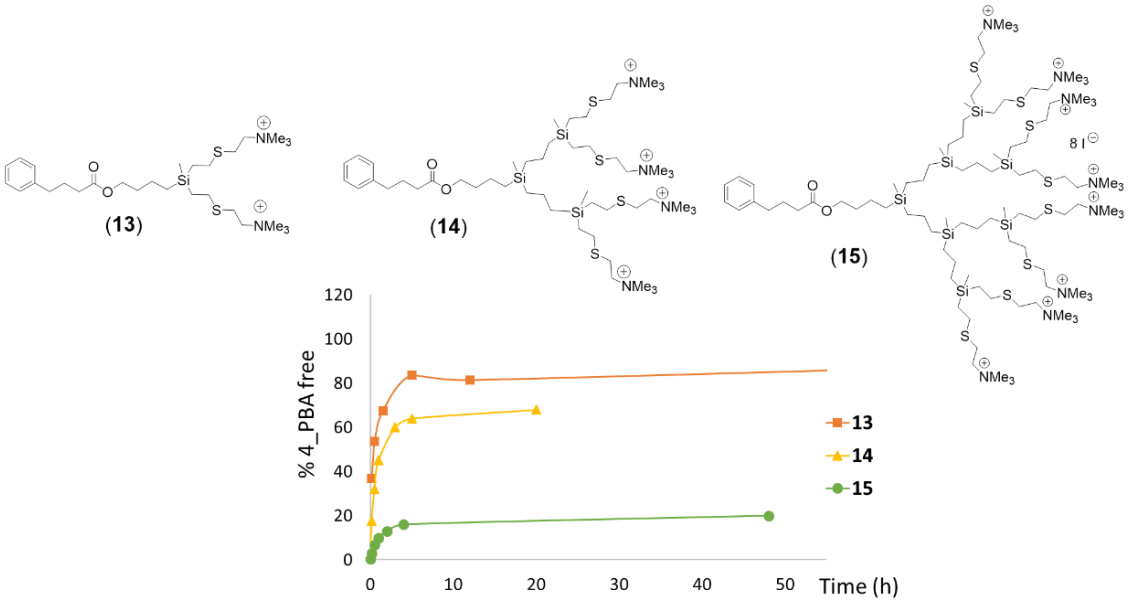

Figure 5. Representative structures of dendronized 4-PBA and their release profile of free chaperone on treatment with pig liver esterase. (1 μmol ester bond: 1 esterase unit. [dendron]=6.9x10^{-4}M).

Study of the anti-amyloid activity of dendrons

Once the influence of the topology on the prevention of IAPP peptide accumulation was proven and the dendritic wedges were functionalized with 4-PBA, the optimal therapeutic dose that would not compromise the viability and functionality of the pancreatic islets was established.

Cell viability was measure by MTT assay in MIN6 cell line treated with $HOC_6H_4OG_3(SNMe_3I)_8$ (**II**) and $ArCO_2G_3(SNMe_3I)_8$ (**15**) under standard culture conditions. The results showed that cell viability was dose-dependent and concentrations higher than 1 μM for **15** and 100 nM for **II** compromised cell viability in the studied cell line (see **Figure 6**).

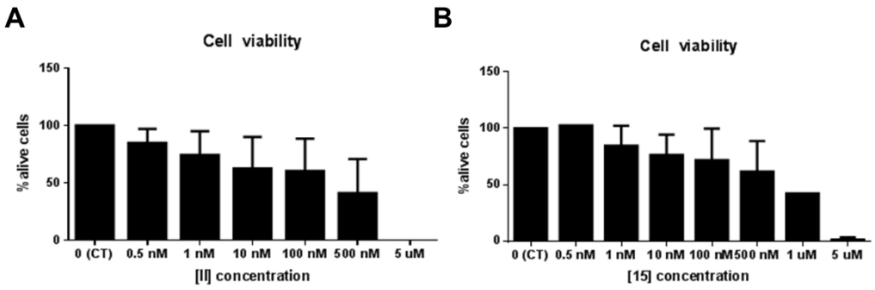

Figure 6. MTT assay on the MIN6 cell line. % of living cells after 7 days of treatment with A) **II** and B) **15** in relation to a control of untreated cells**.**

According to these data, the pancreatic islets isolated from Tg-hIAPP mice of 10-12 weeks aged were treated with a harmless concentration, established at 10 nM for both compounds, during 7

days under high glucose conditions (HG = 16.7 mM). The severity of amyloid formed was observed under the Leica TCS SPE confocal microscope and quantification carried out using the free *Image J* program. The results derived from two independent experiments indicated that **II** and **15**, in a single dose of 10 nM, induced a higher reduction, 76% and 64% respectively, in amyloid severity of pancreatic islets to prevent the amyloid formation (see **Figure 7**). Previous studies showed that 4-PBA at 2.5 mM doses was able to reduce islet amyloid severity in a 43% when islets were treated with free PBA under high glucose conditions.[14] Therefore, in view of the results obtained for dendritic systems, the presence of cationic dendrons affords a higher reduction in the amyloid severity of the amyloid, depending on the focal point, with a single dose five order of magnitude lower than observed for the free 4-PBA (nanomolar vs millimolar concentrations).

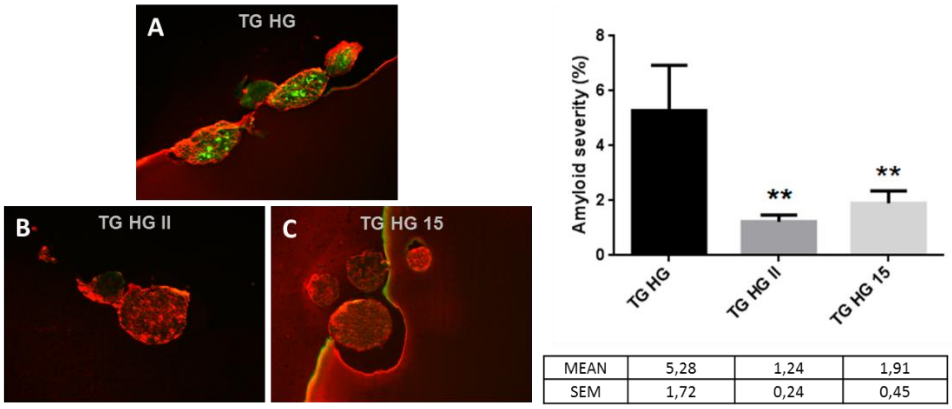

MEAN	5,28	1,24	1,91
SEM	1,72	0,24	0,45

Fig. 7. Amyloid severity reverted by the dendrons. Tg-hIAPP islets in high-glucose conditions (HG, 16.7 mM glucose) during 7 days: A) untreated, B) treated with **II**, C) treated with **15**. Amyloid was determined by fluorescence; in red, insulin (pancreatic islet immunohistochemistry) and in green, thioflavin (amyloid staining). In the right panel, quantification of amyloid severity with the different compounds (**II** and **15**).

The next step, before considering the dendritic compounds as a new anti-amyloid agents, was to evaluate the effect of the presence of dendritic systems in the insulin production by β-cells in pancreatic islets. Insufficient secretion of insulin from the β-cells might lead to pre-diabetes and over frank type 2 diabetes, leading to serious cardiovascular events as a major chronic complications of the disease. The functionality of the islets was determined by an insulin secretion test stimulated by glucose (GSIS), in which the islets of wild type mice (WT) and Tg-hIAPP mice were incubated at low (2.8 mM) and high glucose (16.7 mM) concentration in presence of the dendritic wedges **II** and **15**. At 10 nM, the compounds **II** and **15** did not significant affect the insulin content of the pancreatic islets (**Figure 8A**). However, the insulin secretion in response to glucose was totally blunted in islets treated with compound **II**, from

both wild type and Tg-hIAPP animals, since they did not present a significant increase in the percentage of insulin secreted at 16.7 mM glucose compared to 2.8 mM glucose (**Figure 8B**). Nevertheless, islets cultured with compound **15** maintained a good response of insulin secretion when exposed to high glucose challenge (16.7 mM). This result along with his high anti-amyloid activity could be considered a proof of concept to use the dendron **15** as a potent anti-amyloid agent.

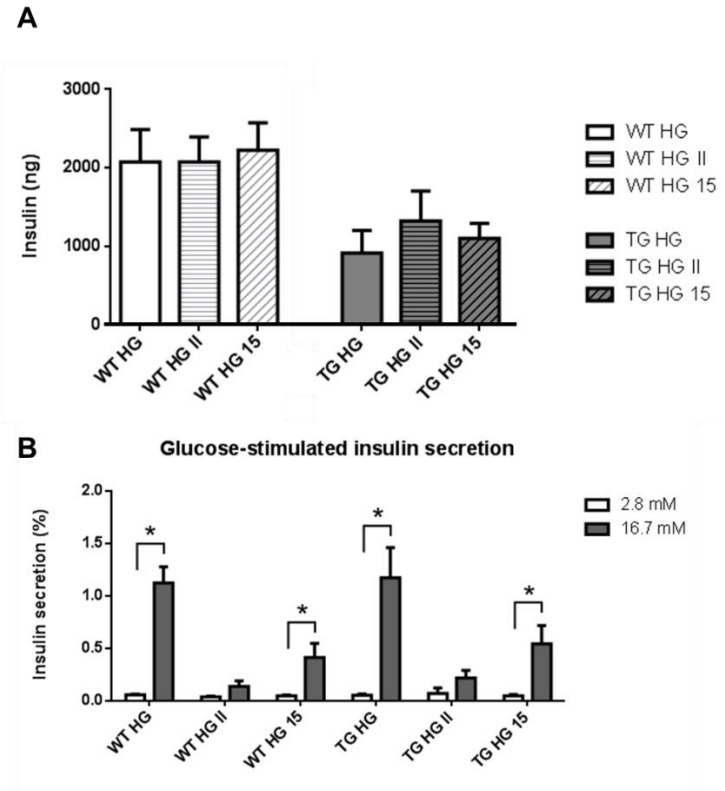

Fig. 8. Pancreatic islet insulin secretion. (A) Insulin content and (B) percentage of insulin secretion respect to insulin content using two different dendrons (**II** and **15**) to determine the functionality of the pancreatic islets at basal condition (2.8 mM glucose) and insulin-stimulating condition (16.7 mM glucose). Results are presented as mean ± SEM. n= 6 batches of eight islets. *p<0.05

Molecular dynamics simulation was performed to identify the structural impact of the dendron binding to IAPP, as well as to evaluate the conformational behaviour of IAPP peptide and the residues involved in the main interactions of the complex. This analysis can be used to better understand how the nature of complex influences in the anti-amyloid biological activity. The simulation study conducted for dendron **15** containing 4-PBA at the focal point showed a strong interaction with the polar residues Asn21 and Asn22 and with the hydrophobic residues Ala25, Ile26 and Leu27 during ~100% of the simulation time (see **Figure 9**) with a free energy value of -11,0 Kcal/mol. This strong interaction is ascribed to the presence of the 4-PBA fragment that

supports and guides the interaction with the folding region through hydrophobic and electrostatic interactions. Hence, MD simulation suggests that chaperon-dendron inhibit IAPP aggregation by a diminution of the inter-peptide association, thereby reducing the probability for the amylin peptides to induce the formation of aggregates,

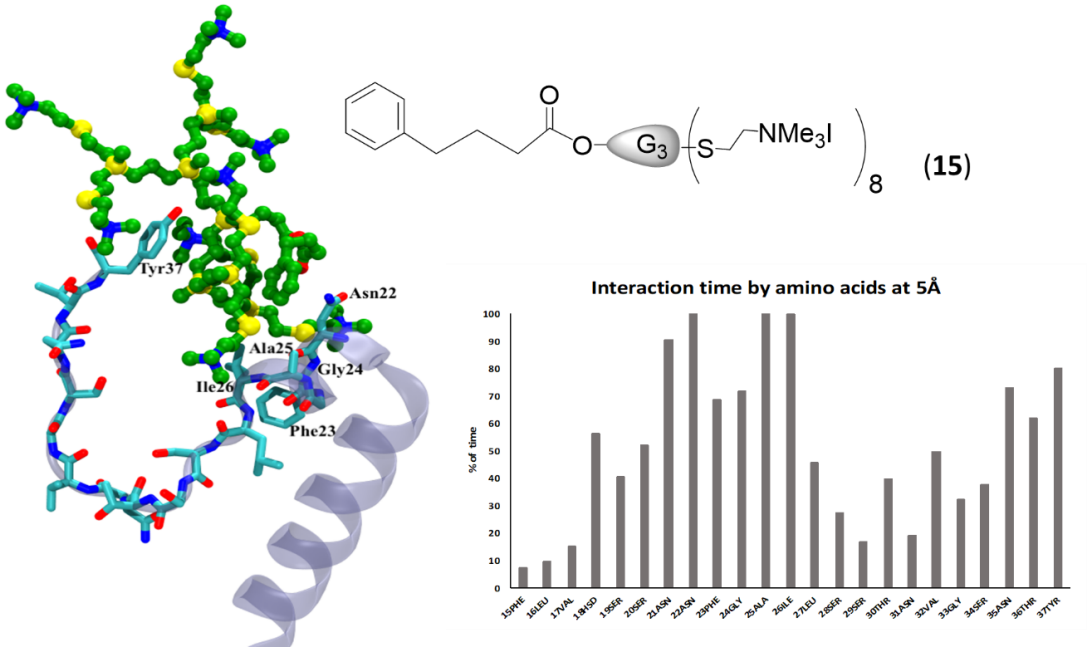

(15)

Fig. 9. Molecular modelling of dendron containing the chaperone 4-PBA at the focal point and the analysis of the interaction with amylin peptide.

CONCLUSIONS

In summary, in this work we combined a simulation method and an experimental approach to determine how the topology of dendrimers influences in their therapeutic action. We synthetized and characterized different topologies of carbosilane cationic systems and tested their anti-amyloid capacity in an animal model of Type 2 Diabetes (T2D). All systems, except globular, prevent or inhibits the formation of amyloid polypeptide (IAPP) deposits in pancreatic islets isolated from Tg-hIAPP mice. Moreover, the dendritic wedges (**II** and **15**) showed the best results when used in a single dose of 10 nM inducing a reduction in amyloid severity of pancreatic islets.

The decrease of the therapeutic dose to obtain the same reduction of amyloid severity, from nanomolar to millimolar, when pancreatic islets were treated with dendritic wedges in relation to free PBA indicates that the presence of the cationic carbosilane wedge determines the high activity of the new systems. However, to keep on the same activity, the dendron **II** negatively affects insulin secretion in both WT and Tg-hIAPP animals, while the dendron functionalized

with 4-PBA (**15**) did not significant affect the insulin secretion of the pancreatic islets. Computational studies carried out to understand at the atomic level the main interaction between IAPP and dendrimers supported the experimental work and determined that the presence of the 4-PBA fragment could guide the interaction with the folding region of IAPP through hydrophobic and electrostatic interactions. This effect provokes a reduction of the inter-peptide association, reducing the probability to form aggregates. All data showed here indicate that the dendron **15** can be considered as dendronized chemical chaperone and new and promising anti-amyloid agent in the treatment of T2D.

EXPERIMENTAL SECTION

Preparation of Dendritic Systems.

Solvents were purified from appropriate drying agents when necessary. Unless otherwise specified, the chemicals were purchased from commercial sources and used as received. *Elemental analysis*. The quantitative analysis of carbon, hydrogen and nitrogen of the described derivatives were carried out in a LECO CHNS-932 microanalyzer. *Nuclear magnetic resonance*. ^{1}H, and ^{13}C NMR assays were performed on Varian spectrometers Unity-300 and Mercury-300. Two-dimensional spectra HSQC {^{1}H-^{13}C}, HMBC{^{1}H-^{29}Si}, HMBC{^{1}H-^{15}N}, TOCSY and DOSY-2D diffusion experiments were performed at 25ºC in a Bruker AV400 or Unity-500 spectrometer. The chemical shifts (ppm) were measured relative to the residual signal of ^{1}H and ^{13}C of the deuterated solvents, in the spectra of ^{29}Si tetramethylsilane (TMS) was taken as reference and in those of ^{15}N nitromethane (CH_3NO_2). *Mass spectrometry*. The different compounds were analysed by means of the ionization technique ESI-TOF-POS in a Bruker Ultraflex III instrument. Reflector mode registrations were made from 450 to 5000 uma.

Synthesis of $V_2G_1[OC_6H_4O]G_1V_2$ (**1**)

A mixture of dendron BrG_2V_4 (**IV**)[28] (0.79 g, 1.73 mmol), hydroquinone (0.09 g, 0.82 mmol), K_2CO_3 (0.45 g, 3.28 mmol) and crown ether (0.082 equivalents) in acetone was stirred at 90°C for 24 hours. Then, the solution was filtered and the solvent evaporated at reduced pressure. The oil obtained was extracted with hexane, and the organic phase dried with $MgSO_4$, and SiO_2 added to remove the crown ether. The solution was filtered and the solvent removed under vacuum. Finally, purification was performed using a size exclusion chromatographic column, obtaining the final compound as a yellow oil (0.29 g, 52%). Data for **1** are as follows. **^{1}H-NMR ($CDCl_3$):** δ (ppm) -0.09 (s, 6H, SiC*H*$_3$), 0.11 (s, 12H, Si(C*H*$_3$)CH=CH$_2$), 0.54 (m, 12H, OCH$_2$CH$_2$CH$_2$C*H*$_2$SiC*H*$_2$) 0.71 (m, 8H, C*H*$_2$SiCH=CH$_2$), 1.50 (m, 12H, SiCH$_2$C*H*$_2$CH$_2$Si, OCH$_2$CH$_2$C*H*$_2$CH$_2$Si), 1.78 (m, 4H, OCH$_2$C*H*$_2$CH$_2$CH$_2$Si), 3.88 (t, 4H, OC*H*$_2$CH$_2$CH$_2$CH$_2$Si), 5.70 (m, 8H, C*H*=CH$_2$), 6.02 (m, 16H, CH=C*H*$_2$), 6.80 (s, 4H, C$_6$*H*$_4$). **^{13}C{^{1}H}-NMR($CDCl_3$):** δ (ppm) -5.5 (Si*C*H$_3$), 13.6 (OCH$_2$CH$_2$CH$_2$*C*H$_2$Si), 18.2-18.8 (Si*C*H$_2$*C*H$_2$*C*H$_2$Si), 20.3

($OCH_2CH_2CH_2CH_2Si$), 33.2 ($OCH_2CH_2CH_2CH_2Si$), 68.2 ($OCH_2CH_2CH_2CH_2Si$), 115.4 (C_6H_4), 132.9 ($CH=CH_2$), 136.7 ($CH=CH_2$), 153.8 (C_{ipso}). **{^{1}H-^{29}Si} HMBC (DMSO-*d*$_6$):** δ (ppm) -13.0 ($Si(CH_3)CH=CH2$), 1.8 ($SiCH_3$). **Elemental analysis (%):** Calc. $C_{48}H_{86}O_2Si_6$ (863.71 g mol^{-1}): C, 66.75; H, 10.04. Found.: C, 66.93; H, 9.61. **MS:** $[M+H]^+$ = 863.53 uma (Calc. 863.52 uma).

Synthesis of $(ClMe_2HNS)_4G_2[OC_6H_4O]G_2(SNHMe_2Cl)_4$ (2)

Compound **1** (0.50 g, 0.58 mmol), 2-(dimethylamino)ethanethiol hydrochloride (0.68 g, 4.84 mmol), 5 mol % of DMPA (0.12 g, 0.48 mmol), and a 1/2 THF/methanol solution (5 mL) were combined. The reaction mixture was deoxygenated and irradiated for 1.5 h. Another 5 mol % of DMPA was added, and the reaction mixture irradiated for another 1.5 h and monitored by ^{1}H NMR. The initial reaction mixture was concentrated by rotary evaporation and redissolved in water. Afterward, the purification was performed using a size exclusion chromatographic column, obtaining the final compound as a yellow solid (0.84 g, 73%). Data for **2** are as follow: **^{1}H-NMR ($CDCl_3$):** δ (ppm) -0.07 (s, 6H, $SiCH_3$), 0.02 (s, 12H, $Si(CH_3)CH_2CH_2S$), 0.58 (m, 20H, $SiCH_2CH_2CH_2Si$, $OCH_2CH_2CH_2CH_2Si$), 0.86 (m, 16H, $SiCH_2CH_2S$), 1.31 (m, 12H, $SiCH_2CH_2CH_2Si$, $OCH_2CH_2CH_2CH_2Si$), 1.68 (m, 4H, $OCH_2CH_2CH_2CH_2Si$), 2.60 (m, 16H, $SiCH_2CH_2S$), 2.70 (s, 48H, $NH(CH_3)_2$), 2.86 (m, 16H, SCH_2CH_2N), 3.21 (m, 16H, SCH_2CH_2N), 3.86 (t, 4H, $OCH_2CH_2CH_2CH_2Si$), 6.81 (s, 4H, C_6H_4). **^{13}C{1H}-NMR($CDCl_3$):** δ (ppm) -5.4 ($SiCH_3$), -5.4 ($Si(CH_3)CH_2CH_2S$), 12.8 ($OCH_2CH_2CH_2CH_2Si$), 13.5 ($SiCH_2CH_2S$), 17.4-17.6 ($SiCH_2CH_2CH_2Si$), 19.6 ($OCH_2CH_2CH_2CH_2Si$), 24.1 (SCH_2CH_2N), 26.2 ($SiCH_2CH_2S$), 32.3 ($OCH_2CH_2CH_2CH_2Si$), 41.4 ($NH(CH_3)_2$), 55.2 (SCH_2CH_2N), 67.0 ($OCH_2CH_2CH_2CH_2Si$), 114.7 (C_6H_4), 152.1 (C_{ipso}). **{^{1}H-^{29}Si} HMBC (DMSO-*d*$_6$):** δ (ppm) 1.0-3.0 ($SiCH_3$). **{^{1}H-^{15}N}-HMBC(DMSO-*d*$_6$):** δ (ppm) -338.2 ($NH(CH_3)_2$). **Elemental analysis (%):** Calc. $C_{80}H_{182}Cl_8N_8O_2S_8Si_6$ (1997.01 g mol^{-1}): C, 48.11; H, 9.19; N, 5.61; S, 12.85. Found: C, 48.15; H, 9.15; N, 5.60; S, 12.83.

Synthesis of $(IMe_3NS)_4G_2[OC_6H_4O]G_2(SNMe_3I)_4$ (3)

A solution of compound **2** (0.27 g, 0.14 mmol) in H_2O/CH_2Cl_2 (1:1) 0.15 g of Na_2CO_3 (1.43 mmol) was added. Once the reaction mixture was maintained for 15 minutes with constant agitation, the organic phase was separated and dried with $MgSO_4$. Finally, the solvent was removed under vacuum to obtain the neutral compound $(Me_2NS)_4G_2[OC_6H_4O]G_2(SNMe_2)_4$ (0.21 g, 91%). Compound **3** was obtained by addition of 0.08 mL CH_3I(1.28 mmol) over a solution of 0.14 g to the neutral compound (0.08 mmol) under inert atmosphere. The reaction was kept under agitation and at room temperature for 18 hours. Subsequently, the volatile components were removed under vacuum and the precipitate was washed with THF, obtaining compound **3** as yellow solid (0.21 g, 96%). Data for **3** are as follow: **^{1}H-NMR ($CDCl_3$):** δ (ppm) -0.07 (s, 6H, $SiCH_3$), 0.03 (s, 12H, $Si(CH_3)CH_2CH_2S$), 0.59 (m, 20H, $SiCH_2CH_2CH_2Si$, $OCH_2CH_2CH_2CH_2Si$), 0.89 (m, 16H, $SiCH_2CH_2S$), 1.33 (m, 12H, $SiCH_2CH_2CH_2Si$,

$OCH_2CH_2CH_2CH_2Si$), 1.68 (m, 4H, $OCH_2CH_2CH_2CH_2Si$), 2.63 (m, 16H, $SiCH_2CH_2S$), 2.89 (m, 16H, SCH_2CH_2N), 3.09 (s, 72H, $N(CH_3)_3$), 3.57 (m, 16H, SCH_2CH_2N), 3.86 (t, 4H, $OCH_2CH_2CH_2CH_2Si$), 6.81 (s, 4H, C_6H_4). **^{13}C{1H}-NMR($CDCl_3$):** δ (ppm) -5.6 ($SiCH_3$), 12.8 ($OCH_2CH_2CH_2CH_2Si$), 13.6 ($SiCH_2CH_2S$), 17.0-17.8 ($SiCH_2CH_2CH_2Si$), 19.6 ($OCH_2CH_2CH_2CH_2Si$), 23.1 (SCH_2CH_2N), 26.3 ($SiCH_2CH_2S$), 32.5 ($OCH_2CH_2CH_2CH_2Si$), 51.6 ($N(CH_3)_3$), 64.0 (SCH_2CH_2N), 67.0 ($OCH_2CH_2CH_2CH_2Si$), 114.6 (C_6H_4), 152.4 (C_{ipso}). **{^{29}Si-^{1}H} HMBC ($CDCl_3$):** δ (ppm) 2.8 ($SiCH_3$). **{^{29}Si-^{15}N} HMBC ($CDCl_3$):** δ (ppm) -329.3 ($N(CH_3)_2$). **Elemental analysis (%):** Calc. $C_{88}H_{198}I_8N_8O_2S_8Si_6$ (2840.83 g mol^{-1}): C, 37.21; H, 7.03; N, 3.94; S, 9.03. Found.: C, 37.46; H, 7.06; N, 3.90; S, 9.05.

Synthesis of $ArCO_2G_1V_2$ (4)

A solution of dendron **III**[28] (0.44 g, 1,87 mmol) and 4-phenyl butyric acid (0.31 g, 1.87 mmol) in acetone (60 mL) was heated to 90 °C in the presence of K_2CO_3(0.39 g, 2.80 mmol) and 18-crown-6 (0.047 g, 0.187 mmol) for 24 h. After this time, volatiles were removed and the mixture was extracted with hexane. The purification was performed using a size exclusion chromatographic column, obtaining the final compound as a yellow oil (0.48 g, 81%). Data for **4** are as follow: **^{1}H-NMR ($CDCl_3$):** δ (ppm) 0.12 (s, 3H, $SiCH_3$), 0.65 (m, 2H, $OCH_2CH_2CH_2CH_2Si$), 1.30 (m, 2H, $OCH_2CH_2CH_2CH_2Si$), 1.63 (m, 2H, $OCH_2CH_2CH_2CH_2Si$), 1.93 (m, 2H, $ArCH_2CH_2CH_2CO_2$), 2.30 (t, 2H, $ArCH_2CH_2CH_2CO_2$), 2.63 (t, 2H, $ArCH_2CH_2CH_2CO_2$), 4.05 (t, 2H, $OCH_2CH_2CH_2CH_2Si$), 5.70 (m, 2H, $CH=CH_2$), 6.06 (m, 4H, $CH=CH_2$), 7.20 (m, 5H, C_6H_5). **^{13}C{^{1}H}-NMR($CDCl_3$):** δ (ppm) -5.4 ($SiCH_3$), 13.5 ($OCH_2CH_2CH_2CH_2Si$), 20.1 ($OCH_2CH_2CH_2CH_2Si$), 26.5 ($ArCH_2CH_2CH_2CO_2$), 32.1 ($OCH_2CH_2CH_2CH_2Si$), 33.6 ($ArCH_2CH_2CH_2CO_2$), 35.1 ($ArCH_2CH_2CH_2CO_2$), 64.0 ($OCH_2CH_2CH_2CH_2Si$), 126.1-128.6 (C_6H_5), 132.9 ($CH=CH_2$), 133.7 ($CH=CH_2$), 141.3 (C_{ipso}), 173.5 (*C*O). **{^{1}H-^{29}Si} HMBC ($CDCl_3$):** δ (ppm) -13.5 ($SiCH_3$). **Elemental analysis (%):** Calc. $C_{19}H_{28}O_2Si$ (316.51 g mol^{-1}): C, 72.10; H, 8.92. Found.: C, 71.86; H, 8.59. **MS:** $[M+H]^+$ = 317.19 uma (Calc. 317.19 uma).

Synthesis of $ArCO_2G_2V_4$ (5)

This wedge was prepared from dendron **IV**[28] (0.26 g, 0.57 mmol), 4-phenyl butyric acid (0.09 g, 0.57 mmol) and K_2CO_3 (0.12 g, 0.86 mmol) using the preparative procedure for **4**. After purification, the final compound **5** was obtained as a yellow oil (0.25 g, 82%). Data for **5** are as follow: **^{1}H-NMR ($CDCl_3$):** δ (ppm) -0.09 (s, 3H, $SiCH_3$), 0.11 (s, 6H, $Si(CH_3)CH=CH_2$), 0.45-0.65 (m, 10H, $OCH_2CH_2CH_2CH_2Si$, $SiCH_2CH_2CH_2Si$), 1.20-1.34 (m, 6H, $OCH_2CH_2CH_2CH_2Si$, $SiCH_2CH_2CH_2Si$), 1.63 (m, 2H, $OCH_2CH_2CH_2CH_2Si$), 1.93 (m, 2H, $ArCH_2CH_2CH_2CO_2$), 2.30 (t, 2H, $ArCH_2CH_2CH_2CO_2$), 2.63 (t, 2H, $ArCH_2CH_2CH_2CO_2$), 4.05 (t, 2H, $OCH_2CH_2CH_2CH_2Si$), 5.70 (m, 4H, $CH=CH_2$), 6.06 (m, 8H, $CH=CH_2$), 7.20 (m, 5H, C_6H_5). **^{13}C{^{1}H}-NMR($CDCl_3$):** δ (ppm) -5.4 ($SiCH_3$), 13.5 ($OCH_2CH_2CH_2CH_2Si$), 18.2-18.8

(Si*C*H$_2$*C*H$_2$*C*H$_2$Si), 20.0 (OCH$_2$CH$_2$*C*H$_2$CH$_2$Si), 26.5 (ArCH$_2$*C*H$_2$CH$_2$CO$_2$), 32.1 (OCH$_2$*C*H$_2$CH$_2$CH$_2$Si), 33.6 (ArCH$_2$CH$_2$*C*H$_2$CO$_2$), 35.2 (Ar*C*H$_2$CH$_2$CH$_2$CO$_2$), 64.0 (O*C*H$_2$CH$_2$CH$_2$CH$_2$Si), 126.1-128.6 (*C*$_6$H$_5$), 132.9 (CH=*C*H$_2$), 133.7 (*C*H=CH$_2$), 141.3 (*C*$_{ipso}$), 173.4 (*C*O). **{^{1}H-^{29}Si}-HMBC (CDCl$_3$):** δ (ppm) -13.5 (*Si*CH$_3$CH=CH$_2$), 1,6 (*Si*CH$_3$). **Elemental analysis (%):** Calc. C$_{31}$H$_{52}$O$_2$Si$_3$ (541.00 g mol^{-1}): C, 68.82; H, 9.69. Found.: C, 68.24; H, 9.39. **MS:** [M+H]$^+$ = 541.33 uma (Calc. 541.33 uma).

Synthesis of A$_r$CO$_2$G$_3$V$_8$ (6)

This wedge was prepared from dendron **V**[28] (0.13 g, 0.14 mmol), 4-phenyl butyric acid (0.02 g, 0.14 mmol) and K$_2$CO$_3$ (0.03 g, 0.22 mmol) using the preparative procedure for **4**. After purification, the final compound **6** was obtained as a yellow oil (0.12 g, 81%). Data for **6** are as follow: **^{1}H-NMR (CDCl$_3$):** δ (ppm) -0.09 (s, 9H, SiC*H*$_3$), 0.11 (s, 12H, Si(C*H*$_3$)CH=CH$_2$), 0.45-0.63 (m, 26H, OCH$_2$CH$_2$CH$_2$C*H*$_2$Si, SiC*H*$_2$CH$_2$C*H*$_2$Si), 1.20-1.34 (m, 14H, OCH$_2$CH$_2$C*H*$_2$CH$_2$Si, SiCH$_2$C*H*$_2$CH$_2$Si), 1.62 (m, 2H, OCH$_2$C*H*$_2$CH$_2$CH$_2$Si), 1.95 (m, 2H, ArCH$_2$C*H*$_2$CH$_2$CO$_2$), 2.30 (t, 2H, ArCH$_2$CH$_2$C*H*$_2$CO$_2$), 2.63 (t, 2H, ArC*H*$_2$CH$_2$CH$_2$CO$_2$), 4.05 (t, 2H, OC*H*$_2$CH$_2$CH$_2$CH$_2$Si), 5.70 (m, 8H, C*H*=CH$_2$), 6.06 (m, 16H, CH=C*H*$_2$), 7.20 (m, 5H, C$_6$*H*$_5$). **^{13}C{^{1}H}-NMR(CDCl$_3$):** δ (ppm) -5.4 (Si*C*H$_3$), 13.5 (OCH$_2$CH$_2$CH$_2$*C*H$_2$Si), 18.2-18.8 (Si*C*H$_2$*C*H$_2$*C*H$_2$Si), 20.0 (OCH$_2$CH$_2$*C*H$_2$CH$_2$Si), 26.5 (ArCH$_2$*C*H$_2$CH$_2$CO$_2$), 32.1 (OCH$_2$*C*H$_2$CH$_2$CH$_2$Si), 33.6 (ArCH$_2$CH$_2$*C*H$_2$CO$_2$), 35.1 (Ar*C*H$_2$CH$_2$CH$_2$CO$_2$), 64.1 (O*C*H$_2$CH$_2$CH$_2$CH$_2$Si), 126.1-128.5 (*C*$_6$H$_5$), 132.9 (CH=*C*H$_2$), 133.7 (*C*H=CH$_2$), 141.3 (*C*$_{ipso}$), 173.4 (*C*O). **{^{1}H-^{29}Si}HMBC (CDCl$_3$):** δ (ppm) -13.5 (*Si*(CH$_3$)CH=CH$_2$), 1.7 (*Si*CH$_3$). **Elemental analysis (%):** Calc C$_{55}$H$_{100}$O$_2$Si$_7$ (989.98 g mol^{-1}): C, 66.73; H, 10.18. Found.: C, 66.32; H, 9.52. **MS:** [M+H]$^+$ = 989.62 uma (Calc. 989.61 uma).

Synthesis of ArCO$_2$G$_1$(SNHMe$_2$Cl)$_2$ (7)

Compound **7** was prepared using the preparative procedure for **2** starting to **4** (0.42 g, 1.32 mmol), HS(CH$_2$)$_2$SNHMe$_2$Cl (0.38 g, 2.69 mmol) and DMPA (0.07 g, 0.27 mmol). Compound **7** was obtained as a white solid (0.21 g, 26%). Data for **7** are as follow: **^{1}H-NMR (DMSO-*d*$_6$):** δ (ppm) 0.01 (s, 3H, SiC*H*$_3$), 0.55 (m, 2H, OCH$_2$CH$_2$CH$_2$C*H*$_2$Si), 0.85 (m, 4H, SiC*H*$_2$CH$_2$S), 1.28 (m, 2H, OCH$_2$CH$_2$C*H*$_2$CH$_2$Si), 1.55 (m, 2H, OCH$_2$C*H*$_2$CH$_2$CH$_2$Si), 1.80 (m, 2H, ArCH$_2$C*H*$_2$CH$_2$CO$_2$), 2.27 (m, 2H, ArCH$_2$CH$_2$C*H*$_2$CO$_2$), 2.50 (t, 2H, ArC*H*$_2$CH$_2$CH$_2$CO$_2$), 2.60 (m, 4H, SiCH$_2$C*H*$_2$S), 2.70 (s, 12H, NH(C*H*$_3$)$_2$), 2.80 (m , 4H, SC*H*$_2$CH$_2$NH(CH$_3$)$_2$), 3.16 (m, 4H, SCH$_2$C*H*$_2$NH(CH$_3$)$_2$), 3.99 (m, 2H, OC*H*$_2$CH$_2$CH$_2$CH$_2$Si), 7.12-7.28 (m, 5H, C$_6$*H*$_5$). **^{13}C{^{1}H}-NMR(DMSO-*d*$_6$):** δ (ppm) -5.4 (Si*C*H$_3$), 12.5 (OCH$_2$CH$_2$CH$_2$*C*H$_2$Si), 13.5 (SiC*H*$_2$CH$_2$S), 19.4 (OCH$_2$CH$_2$*C*H$_2$CH$_2$Si), 24.7 (S*C*H$_2$CH$_2$NH(CH$_3$)$_2$), 25.9 (ArCH$_2$*C*H$_2$CH$_2$CO$_2$), 26.0 (SiCH$_2$*C*H$_2$S), 31.4 (OCH$_2$*C*H$_2$CH$_2$CH$_2$Si), 32.5 (ArCH$_2$CH$_2$*C*H$_2$CO$_2$), 33.8 (Ar*C*H$_2$CH$_2$CH$_2$CO$_2$), 41.4 (NH(*C*H$_3$)$_2$), 55.3 (SCH$_2$*C*H$_2$NH(CH$_3$)$_2$), 62.8 (O*C*H$_2$CH$_2$CH$_2$CH$_2$Si), 125.37 y 127.8 (*C*$_6$H$_5$), 140.8 (*C*$_{ipso}$), 172.1 (*C*O). **{^{1}H-^{29}Si} HMBC**

(DMSO-d_6): δ (ppm) 3.0 (*Si*CH_3). **{^{1}H-^{15}N}-HMBC(DMSO-d_6):** δ (ppm) -339.1 (*N*H*(*$CH_3)_2$). **Elemental analysis (%):** Calc. $C_{27}H_{52}Cl_2N_2O_2S_2Si$ (599.83 g mol^{-1}): C, 54.06; H, 8.74; N, 4.67.Found.: C, 54.72; H, 8.81; N, 4.65.

Synthesis of $ArCO_2G_2(SNHMe_2Cl)_4$ (8)

Compound **8** was prepared using the preparative procedure for **2** starting to **5** (0.13 g, 0.24 mmol), $HS(CH_2)_2SNHMe_2Cl$ (0.14 g, 0.97 mmol) and DMPA (0.03 g, 0.10 mmol). Compound **8** was obtained as a white solid (0.19 g, 73%). Data for **8** are as follow: **^{1}H-NMR (DMSO-d_6):** δ (ppm) -0.09 (s, 3H, SiC*H*$_3$), 0.01 (s, 6H, Si(C*H*$_3$)CH_2CH_2S), 0.50-0.63 (m, 10H, $OCH_2CH_2CH_2CH_2Si$, $SiCH_2CH_2CH_2Si$), 0.87 (m, 8H, $SiCH_2CH_2S$), 1.22-1.35 (m, 6H, $OCH_2CH_2CH_2CH_2Si$, $SiCH_2CH_2CH_2Si$), 1.55 (m, 2H, $OCH_2CH_2CH_2CH_2Si$), 1.80 (m, 2H, $ArCH_2CH_2CH_2CO_2$), 2.27 (m, 2H, $ArCH_2CH_2CH_2CO_2$), 2.50 (t, 2H, $ArCH_2CH_2CH_2CO_2$), 2.60 (m, 8H, $SiCH_2CH_2S$), 2.70 (s, 24H, $NH(CH_3)_2$), 2.80 (m , 8H, $SCH_2CH_2NH(CH_3)_2$), 3.16 (m, 8H, $SCH_2CH_2NH(CH_3)_2$), 3.99 (m, 2H, $OCH_2CH_2CH_2CH_2Si$), 7.12-7.28 (m, 5H, C_6H_5). **^{13}C{^{1}H}-NMR(DMSO-d_6):** δ (ppm) -5.7 ($SiCH_3$), 12.5 ($OCH_2CH_2CH_2CH_2Si$), 13.5 ($SiCH_2CH_2S$), 17.2-17.5 ($SiCH_2CH_2CH_2Si$), 19.4 ($OCH_2CH_2CH_2CH_2Si$), 24.3 ($SCH_2CH_2NH(CH_3)_2$), 25.9 ($ArCH_2CH_2CH_2CO_2$), 26.0 ($SiCH_2CH_2S$), 31.4 ($OCH_2CH_2CH_2CH_2Si$), 32.5 ($ArCH_2CH_2CH_2CO_2$), 33.8 ($ArCH_2CH_2CH_2CO_2$), 41.4 ($NH(CH_3)_2$), 55.3 ($SCH_2CH_2NH(CH_3)_2$), 62.8 ($OCH_2CH_2CH_2CH_2Si$), 125.37 y 127.8 (C_6H_5), 140.8 (C_{ipso}), 172.1 (*C*O). **{^{1}H-^{29}Si} HMBC (DMSO-d_6):** δ (ppm) 1.8 (*Si*CH_3), 2.7 (*Si*$(CH_3)CH_2CH_2S$). **{^{1}H-^{15}N}-HMBC(DMSO-d_6):** δ (ppm) -339.1 (*N*H*(*$CH_3)_2$). **Elemental analysis (%):** Calc. para $C_{47}H_{100}Cl_4N_4O_2S_4Si_3$ (1107.64 g mol^{-1}): C, 50.97; H, 9.10; N, 5.06. Found.: C, 50.61; H, 9.03; N, 5.03.

Synthesis of $ArCO_2G_3(SNHMe_2Cl)_8$ (9)

Compound **9** was prepared using the preparative procedure for **2** starting to **6** (0.16 g, 0.16 mmol), $HS(CH_2)_2SNHMe_2Cl$ (0.18 g, 1.32 mmol) and DMPA (0.03 g, 0.13 mmol). Compound **9** was obtained as a white solid (0.27 g, 81%). Data for **9** are as follow: **^{1}H-NMR (DMSO-d_6):** δ (ppm) -0.09 (s, 9H, SiC*H*$_3$), 0.01 (s, 12H, Si(C*H*$_3$)CH_2CH_2S), 0.50-0.63 (m, 26H, $OCH_2CH_2CH_2CH_2Si$, $SiCH_2CH_2CH_2Si$), 0.87 (m, 16H, $SiCH_2CH_2S$), 1.22-1.35 (m, 14H, $OCH_2CH_2CH_2CH_2Si$, $SiCH_2CH_2CH_2Si$), 1.55 (m, 2H, $OCH_2CH_2CH_2CH_2Si$), 1.80 (m, 2H, $ArCH_2CH_2CH_2CO_2$), 2.29 (m, 2H, $ArCH_2CH_2CH_2CO_2$), 2.50 (t, 2H, $ArCH_2CH_2CH_2CO_2$), 2.60 (m, 16H, $SiCH_2CH_2S$), 2.72 (s, 48H, $NH(CH_3)_2$), 2.80 (m , 16H, $SCH_2CH_2NH(CH_3)_2$), 3.16 (m, 16H, $SCH_2CH_2NH(CH_3)_2$), 3.99 (m, 2H, $OCH_2CH_2CH_2CH_2Si$), 7.12-7.28 (m, 5H, C_6H_5). **^{13}C{^{1}H}-NMR(DMSO-d_6):** δ (ppm) -5.7 ($SiCH_3$), 12.5 ($OCH_2CH_2CH_2CH_2Si$), 13.5 ($SiCH_2CH_2S$), 17.1-17.5 ($SiCH_2CH_2CH_2Si$), 19.4 ($OCH_2CH_2CH_2CH_2Si$), 24.3 ($SCH_2CH_2NH(CH_3)_2$), 25.9 ($ArCH_2CH_2CH_2CO_2$), 26.1 ($SiCH_2CH_2S$), 31.4 ($OCH_2CH_2CH_2CH_2Si$), 32.5 ($ArCH_2CH_2CH_2CO_2$), 33.8 ($ArCH_2CH_2CH_2CO_2$), 41.4

(NH(CH$_3$)$_2$), 55.3 (SCH$_2$$CH_2$NH(CH$_3$)$_2$), 62.8 (O$CH_2CH_2CH_2CH_2$Si), 125.37 y 127.8 ($C_6H_5$), 140.8 ($C_{ipso}$), 172.1 ($C$O). **{^{1}H-^{29}Si} HMBC (DMSO-d_6):** δ (ppm) 1.8 (SiCH$_3$), 2.7 (Si(CH$_3$)CH$_2$CH$_2$S). **{^{1}H-^{15}N}-HMBC(DMSO-d_6):** δ (ppm) -338.3 (NH(CH$_3$)$_2$). **Elemental analysis (%):** Calc. $C_{87}H_{196}Cl_8N_8O_2S_8Si_7$ (2123.25 g mol^{-1}): C, 49.21; H, 9.30; N, 5.28. Found.: C, 49.78; H, 9.13; N, 5.37.

Synthesis of ArCO$_2$G$_1$(SNMe$_2$)$_2$ (10)

To a solution of compound **7** (0,163 g, 0,27 mmol) in H$_2$O/CH$_2$Cl$_2$ (1:1) 0.07g of Na$_2$CO$_3$ (0.71 mmol) was added. Once the reaction mixture was maintained for 15 minutes with constant agitation, the organic phase was separated and dried with MgSO$_4$. Finally, the solvent was removed under vacuum to obtain the neutral compound **10** as a yellow oil (0.13 g, 91%). Data for **10** are as follow: **^{1}H-NMR (CDCl$_3$):** δ (ppm) 0.00 (s, 3H, SiCH_3), 0.55 (m, 2H, OCH$_2$CH$_2$CH$_2$CH_2Si), 0.89 (m, 4H, SiCH_2CH$_2$S), 1.33 (m, 2H, OCH$_2$CH$_2$CH_2CH$_2$Si), 1.61 (m, 2H, OCH$_2$CH_2CH$_2$CH$_2$Si), 1.94 (m, 2H, ArCH$_2$CH_2CH$_2$CO$_2$), 2.24 (s, 12H, N(CH_3)$_2$), 2.30 (t, 2H, ArCH$_2$CH$_2$CH_2CO$_2$), 2.45-2.65 (t, 14H, , ArCH_2CH$_2$CH$_2$CO$_2$, SiCH$_2$CH_2S, SCH_2CH_2N), 4.04 (t, 2H, OCH_2CH$_2$CH$_2$CH$_2$Si), 7.20 (m, 5H, C$_6H_5$). **^{13}C{^{1}H}-NMR(CDCl$_3$):** δ (ppm) -5.4 (SiCH$_3$), 13.2 (OCH$_2$CH$_2$CH$_2$$CH_2$Si), 14.4 (Si$CH_2CH_2$S), 20.1 (OCH$_2CH_2$$CH_2CH_2$Si), 26.5 (ArCH$_2$$CH_2CH_2CO_2$), 27.7 (SiCH$_2$$CH_2$S), 29.5 (S$CH_2CH_2$N), 32.3 (OCH$_2$$CH_2CH_2CH_2$Si), 33.6 (ArCH$_2CH_2$$CH_2CO_2$), 35.1 (Ar$CH_2CH_2CH_2CO_2$), 45.3 (N($CH_3$)$_2$), 59.1 (SCH$_2$$CH_2$N), 63.8 (O$CH_2CH_2CH_2CH_2$Si), 128.6 ($C_6H_5$), 141.3 ($C_{ipso}$), 173.5 ($C$O). **{^{1}H-^{29}Si}HMBC (CDCl$_3$):** δ (ppm) 3.0 (SiCH$_3$). **{^{1}H-^{15}N}-HMBC(CDCl$_3$):** δ (ppm) -352.3 (N(CH$_3$)$_2$). **Elemental analysis (%):** Calc. $C_{27}H_{50}N_2O_2S_2Si$ (526.91 g mol^{-1}): C, 61.54; H, 9.56; N, 5.32; S, 12.17. found: C, 61.53; H, 9.28; N, 5.13; S, 12.16. **MS:** [M+H]$^+$ = 527.31 uma (Calc. 527.31 uma).

Synthesis of ArCO$_2$G$_2$(SNMe$_2$)$_4$ (11)

Compound **11** was prepared using the preparative procedure for **10** starting to **8** (0.12 g, 0.11 mmol) and Na$_2$CO$_3$ (0.06 g, 0.55 mmol). Compound **11** was obtained as a yellow oil (0.10 g, 93%). Data for **11** are as follow: **^{1}H-NMR (CDCl$_3$):** δ (ppm) -0.12 (s, 3H, SiCH_3), -0.02 (s, 6H, Si(CH_3)CH$_2$CH$_2$S), 0.49-0.63 (m, 10H, OCH$_2$CH$_2$CH$_2$CH_2Si, SiCH_2CH$_2$CH_2Si), 0.86 (m, 8H, SiCH_2CH$_2$S), 1.23-1.30 (m, 6H, OCH$_2$CH$_2$CH_2CH$_2$Si, SiCH$_2$CH_2CH$_2$Si), 1.61 (m, 2H, OCH$_2$CH_2CH$_2$CH$_2$Si), 1.93 (m, 2H, ArCH$_2$CH_2CH$_2$CO$_2$), 2.24 (s, 24H, N(CH_3)$_2$), 2.30 (t, 2H, ArCH$_2$CH$_2$CH_2CO$_2$), 2.44-2.63 (t, 26H, , ArCH_2CH$_2$CH$_2$CO$_2$, SiCH$_2$CH_2S, SCH_2CH_2N), 4.05 (t, 2H, OCH_2CH$_2$CH$_2$CH$_2$Si), 7.20 (m, 5H, C$_6H_5$). **^{13}C{^{1}H}-NMR(CDCl$_3$):** δ (ppm) -5.4 (SiCH$_3$), -5.7 (Si(CH$_3$)CH$_2$CH$_2$S), 13.5 (OCH$_2$CH$_2$CH$_2$$CH_2$Si), 14.4 (Si$CH_2CH_2$S), 17.3-17.7 (Si$CH_2$$CH_2$$CH_2$Si), 20.1 (OCH$_2CH_2$$CH_2CH_2$Si), 26.5 (ArCH$_2$$CH_2CH_2CO_2$), 27.7 (SiCH$_2$$CH_2$S), 29.5 (S$CH_2CH_2$N), 32.1 (OCH$_2$$CH_2CH_2CH_2$Si), 33.9 (ArCH$_2CH_2$$CH_2CO_2$), 35.1 (Ar$CH_2CH_2CH_2CO_2$), 45.2 (N($CH_3$)$_2$), 59.2 (SCH$_2$$CH_2$N), 64.0 (O$CH_2CH_2CH_2CH_2$Si), 126.1-128.6 ($C_6H_5$), 141.3 ($C_{ipso}$), 173.4 ($C$O). **{^{1}H-^{29}Si} HMBC (CDCl$_3$):** δ (ppm) 1.8 (SiCH$_3$), 2.7

(*Si*(CH_3)CH_2CH_2S). **{^{1}H-^{15}N}-HMBC($CDCl_3$):** δ (ppm) -352.7 (*N*(CH_3)$_2$). **Elemental analysis (%):** Calc. para $C_{47}H_{96}N_4O_2S_4Si_3$ (961.81 g mol^{-1}): C, 58.69; H, 10.06; N, 5.83; S, 13.34. Found.: C, 58.93; H, 9.38; N, 5.33; S, 13.35. **MS:** $[M+H]^+$ = 961.58 uma (Calc. 961.57 uma).

Synthesis of $ArCO_2G_3(SNMe_2)_8$ (12)

Compound **12** was prepared using the preparative procedure for **10** starting to **9** (0.11 g, 0.05 mmol) and Na_2CO_3 (0.06 g, 0.55 mmol). Compound **12** was obtained as a yellow oil (0.09 g, 91%). Data for **12** are as follow: **^{1}H-NMR (DMSO-*d*$_6$):** δ (ppm) -0.12 (s, 9H, SiC*H*$_3$), -0.02 (s, 12H, Si(C*H*$_3$)CH_2CH_2S), 0.49-0.63 (m, 26H, $OCH_2CH_2CH_2CH_2$Si, SiC*H*$_2CH_2CH_2$Si), 0.86 (m, 16H, SiC*H*$_2CH_2$S), 1.23-1.30 (m, 14H, $OCH_2CH_2CH_2CH_2$Si, $SiCH_2CH_2CH_2$Si), 1.61 (m, 2H, $OCH_2CH_2CH_2CH_2$Si), 1.93 (m, 2H, $ArCH_2CH_2CH_2CO_2$), 2.24 (s, 48H, N(C*H*$_3$)$_2$), 2.30 (t, 2H, $ArCH_2CH_2CH_2CO_2$), 2.44-2.63 (t, 50H, , ArC*H*$_2CH_2CH_2CO_2$, $SiCH_2CH_2$S, SC*H*$_2CH_2$N), 4.05 (t, 2H, OC*H*$_2CH_2CH_2CH_2$Si), 7.20 (m, 5H, C_6H_5). **^{13}C{^{1}H}-NMR(DMSO-*d*$_6$):** δ (ppm) -5.4 (Si*C*H_3), -5.7 (Si(*C*H_3)CH_2CH_2S), 13.5 ($OCH_2CH_2CH_2CH_2$Si), 14.4 (Si*C*H_2CH_2S), 17.3-17.7 (Si*C*$H_2CH_2CH_2$Si), 20.1 ($OCH_2CH_2CH_2CH_2$Si), 26.5 ($ArCH_2CH_2CH_2CO_2$), 27.7 ($SiCH_2CH_2$S), 29.4 (S*C*H_2CH_2N), 32.14 ($OCH_2CH_2CH_2CH_2$Si), 33.9 ($ArCH_2CH_2CH_2CO_2$), 35.1 ($ArCH_2CH_2CH_2CO_2$), 45.2 (N(*C*H_3)$_2$), 59.1 (SCH_2CH_2N), 64.0 ($OCH_2CH_2CH_2CH_2$Si), 126.1-128.6 (*C*$_6H_5$), 141.3 (*C*$_{ipso}$), 173,4 (*C*O). **{^{1}H-^{29}Si} HMBC (DMSO-*d*$_6$):** δ (ppm) 1.8 (*Si*CH_3), 2.7 (*Si*(CH_3)CH_2CH_2S). **{^{1}H-^{15}N}-HMBC(DMSO-*d*$_6$):** δ (ppm) -352.7 (*N*(CH_3)$_2$). **Elemental analysis (%):** Calc. para $C_{87}H_{188}N_8O_2S_8Si_7$ (1831.59 g mol^{-1}): C, 57.05; H, 10.35; N, 6.12; S, 14.01. Found.: C, 57.38; H, 9.52; N, 6.18; S, 14.02. **MS:** $[M+H]^+$ = 1831.11 uma (Calc. 1830.10 uma).

Synthesis of $ArCO_2G_1(SNMe_3I)_2$ (13)

Compound **13** was obtained by addition of 0.01 mL CH_3I (0.20 mmol) over a solution of **10** (0.05 g, 0.05 mmol) under inert atmosphere. The reaction was kept under agitation and at room temperature for 18 hours. Subsequently, the volatile components were removed under vacuum and the precipitate washed with THF, obtaining compound **13** as yellow solid (0.02 g, 87%). Data for **13** are as follow: **^{1}H-RMN (DMSO-*d*$_6$):** δ (ppm) 0.02 (s, 3H, SiC*H*$_3$), 0.60 (m, 2H, $OCH_2CH_2CH_2CH_2$Si), 0.85 (m, 4H, SiC*H*$_2CH_2$S), 1.31 (m, 2H, $OCH_2CH_2CH_2CH_2$Si), 1.58 (m, 2H, $OCH_2CH_2CH_2CH_2$Si), 1.80 (m, 2H, $ArCH_2CH_2CH_2CO_2$), 2.30 (t, 2H, $ArCH_2CH_2CH_2CO_2$), 2.41-2.65 (t, 6H, $SiCH_2CH_2$S, ArC*H*$_2CH_2CH_2CO_2$), 2.88 (t, 4H, SC*H*$_2CH_2$N), 3.06 (s, 18H, N(C*H*$_3$)$_3$), 3.49 (t, 4H, SCH_2CH_2N), 4.01 (t, 2H, OC*H*$_2CH_2CH_2CH_2$Si), 7.23 (m, 5H, C_6H_5). **^{13}C{^{1}H}-NMR(DMSO-*d*$_6$):** δ (ppm) -5.3 (Si*C*H_3), 12.5 ($OCH_2CH_2CH_2CH_2$Si), 13.9 (Si*C*H_2CH_2S), 19.6 ($OCH_2CH_2CH_2CH_2$Si), 23.6 (S*C*H_2CH_2N), 26.4 ($SiCH_2CH_2$S), 26.7 ($ArCH_2CH_2CH_2CO_2$) 31.9 ($OCH_2CH_2CH_2CH_2$Si), 32.9 ($ArCH_2CH_2CH_2CO_2$), 34.3 ($ArCH_2CH_2CH_2CO_2$), 52.2 (N(*C*H_3)$_3$), 63.4 (SCH_2CH_2N), 64.5 ($OCH_2CH_2CH_2CH_2$Si), 125.9-

128.4 (C_6H_5), 141.3 (C_{ipso}), 173.8 (CO). **{^{1}H-^{29}Si} HMBC (DMSO-*d*$_6$):** δ (ppm) 3.0 ($SiCH_3$). **{^{1}H-^{15}N}-HMBC(DMSO-*d*$_6$):** δ (ppm) -329.3 ($N(CH_3)_3$). **Elemental analysis (%):** Calc. para $C_{29}H_{56}I_2N_2O_2S_2Si$ (810.79 g mol^{-1}): C, 42.96; H, 6.96; N, 3.46; S, 7,91. Found.: C, 43.08; H, 6.99; N, 3.43; S, 7.95.

Synthesis of $ArCO_2G_2(SNMe_3I)_4$ (14)

Compound **14** was prepared using the preparative procedure for **13** starting to **11** (0.03 g, 0.03 mmol) and CH_3I (0.01 mL, 0.20 mmol). Compound **14** was obtained as a yellow solid (0.09 g, 91%). Data for **14** are as follow: **^{1}H-NMR (DMSO-*d*$_6$):** δ (ppm) -0.10 (s, 3H, $SiCH_3$), 0,01 (s, 6H, $Si(CH_3)CH_2CH_2S$), 0.48-0.61 (m, 10H, $OCH_2CH_2CH_2CH_2Si$, $SiCH_2CH_2CH_2Si$), 0.85 (m, 8H, $SiCH_2CH_2S$), 1.31 (m, 6H, $OCH_2CH_2CH_2CH_2Si$, $SiCH_2CH_2CH_2Si$), 1.58 (m, 2H, $OCH_2CH_2CH_2CH_2Si$), 1.80 (m, 2H, $ArCH_2CH_2CH_2CO_2$), 2.30 (t, 2H, $ArCH_2CH_2CH_2CO_2$), 2.45-2.61 (t, 10H, $SiCH_2CH_2S$, $ArCH_2CH_2CH_2CO_2$), 2.88 (t, 8H, SCH_2CH_2N), 3.06 (s, 36H, $N(CH_3)_3$), 3.49 (t, 8H, SCH_2CH_2N), 4.01 (t, 2H, $OCH_2CH_2CH_2CH_2Si$), 7.23 (m, 5H, C_6H_5). **^{13}C{^{1}H}-NMR(DMSO-*d*$_6$):** δ (ppm) -5.3 ($SiCH_3$), 12.5 ($OCH_2CH_2CH_2CH_2Si$), 13.9 ($SiCH_2CH_2S$), 17.3-17.9 ($SiCH_2CH_2CH_2Si$), 19.6 ($OCH_2CH_2CH_2CH_2Si$), 23.5 (SCH_2CH_2N), 26.5 ($SiCH_2CH_2S$), 26.7 ($ArCH_2CH_2CH_2CO_2$) 31.9 ($OCH_2CH_2CH_2CH_2Si$), 32.9 ($ArCH_2CH_2CH_2CO_2$), 34.4 ($ArCH_2CH_2CH_2CO_2$), 52.1 ($N(CH_3)_3$), 63.4 (SCH_2CH_2N), 64.5 ($OCH_2CH_2CH_2CH_2Si$), 125.9-128.4 (C_6H_5), 141.3 (C_{ipso}), 173.8 (CO). **{^{1}H-^{29}Si} HMBC (DMSO-*d*$_6$):** δ (ppm) 1.1 ($SiCH_3$), 3.0 ($Si(CH_3)CH_2CH_2S$). **{^{1}H-^{15}N}-HMBC(DMSO-*d*$_6$):** δ (ppm) -329.5 ($N(CH_3)_3$). **Elemental analysis (%):** Calc. $C_{51}H_{108}I_4N_4O_2S_4Si_3$ (1529.56 g mol^{-1}): C, 40.05; H, 7.12; N, 3.66; S, 8.39. Found: C, 40,00; H, 7.13; N, 3.67; S, 8.37.

Synthesis of $ArCO_2G_3(SNMe_3I)_8$ (15)

Compound **15** was prepared using the preparative procedure for **13** starting to **12** (0.05 g, 0.02 mmol) and CH_3I (0.02 mL, 0.39 mmol). Compound **15** was obtained as a yellow solid (0.06 g, 87%). Data for **15** are as follow: **^{1}H-NMR (DMSO-*d*$_6$):** δ (ppm) -0.10 (s, 9H, $SiCH_3$), 0.01 (s, 12H, $Si(CH_3)CH_2CH_2S$), 0.48-0.61 (m, 26H, $OCH_2CH_2CH_2CH_2Si$, $SiCH_2CH_2CH_2Si$), 0.85 (m, 16H, $SiCH_2CH_2S$), 1.21-1.40 (m, 14H, $OCH_2CH_2CH_2CH_2Si$, $SiCH_2CH_2CH_2Si$), 1.58 (m, 2H, $OCH_2CH_2CH_2CH_2Si$), 1.80 (m, 2H, $ArCH_2CH_2CH_2CO_2$), 2.30 (t, 2H, $ArCH_2CH_2CH_2CO_2$), 2.40-2.60 (t, 18H, $SiCH_2CH_2S$, $ArCH_2CH_2CH_2CO_2$), 2.88 (t, 16H, SCH_2CH_2N), 3,06 (s, 72H, $N(CH_3)_3$), 3.49 (t, 16H, SCH_2CH_2N), 4.01 (t, 2H, $OCH_2CH_2CH_2CH_2Si$), 7.23 (m, 5H, C_6H_5). **^{13}C{^{1}H}-NMR(DMSO-*d*$_6$):** δ (ppm) -5.4 ($SiCH_3$), 12.5 ($OCH_2CH_2CH_2CH_2Si$), 13.9 ($SiCH_2CH_2S$), 17.3-17.9 ($SiCH_2CH_2CH_2Si$), 19.6 ($OCH_2CH_2CH_2CH_2Si$), 23.4 (SCH_2CH_2N), 26.5 ($SiCH_2CH_2S$), 26.7 ($ArCH_2CH_2CH_2CO_2$) 31.9 ($OCH_2CH_2CH_2CH_2Si$), 32.9 ($ArCH_2CH_2CH_2CO_2$), 34.4 ($ArCH_2CH_2CH_2CO_2$), 52.1 ($N(CH_3)_3$), 63.4 (SCH_2CH_2N), 64.5 ($OCH_2CH_2CH_2CH_2Si$), 125.9-128.4 (C_6H_5), 141.3 (C_{ipso}), 173.8 (CO). **{^{1}H-^{29}Si} HMBC (DMSO-*d*$_6$):** δ (ppm) 1.0 ($SiCH_3$), 3.0 ($Si(CH_3)CH_2CH_2S$). **{^{1}H-^{15}N}-HMBC(DMSO-*d*$_6$):** δ

(ppm) -329.2 (*N*(CH_3)$_3$). **Elemental analysis (%):** Calc. para $C_{95}H_{212}I_8N_8O_2S_8Si_7$ (2967.10 g mol^{-1}): C, 38.46; H, 7.20; N, 3.78; S, 8.65. Exp.: C, 38.49; H, 7.16; N, 3.80; S, 8.64.

Islet isolation and culture.

Mouse pancreatic islets were isolated from 10-12 weeks old wild type (WT) and Tg-hIAPP male mice by collagenase perfusion and digestion and Histopaque gradient (Sigma-Aldrich) as described elsewhere.[14] Islets were allowed to recover for 24h at 37ºC and 5% CO_2 in RPMI 1640 medium (11.1 mM glucose) supplemented with 10% foetal bovine serum (FBS) (v/v), 2 mM L-glutamine, 100 U/mL penicillin and 100 mg/mL streptomycin.

For amyloid formation experiments, islets were cultured together with the dendritic compounds at the indicated doses for 7 days under high glucose conditions (HG= 16.7 mM). The viability of pancreatic islets was analysed by microscopic loupe counting in relation to the initial number of islets at the beginning of the treatment.

Amyloid formation

For double insulin and amyloid (thioflavin S) staining, isolated pancreatic islets were embedded in 2% agarose. Pancreatic islets sections were then fixed with 4%paraformaldehyde (Sigma-Aldrich) for 10 min. After blocking with PBS in 10% foetal bovine serum and 0.5% Triton X-100 (Sigma-Aldrich), islets were incubated with polyclonal guinea pig anti-insulin (Dako, Glostrup, Denmark) followed by secondary incubation with Alexa Fluor 555 conjugated goat anti–guinea pig IgG (Life Technologies, Carlsbad, CA, USA). Sections were then incubated in 0.5% thioflavin S (Sigma-Aldrich) solution for 2 min and rinsed twice with 70% ethanol.

Fluorescent slides were viewed using a Leica TCS SPE confocal microscope (Leica Microsystems, Buffalo Grove, IL, USA), and images were acquired using Leica LAS Image Analysis software. A minimum of 25 images per condition were quantified using the free *Image J* program.

MIN6 cell line culture

Mouse pancreatic cell line MIN6, derived from *in vivo* immortalized insulin secreting pancreatic β cells, was maintained in DMEM (Sigma-Aldrich) containing 25 mM glucose and supplemented with 10% FBS (vol/vol), 2 mM L-glutamine, 100 U/mL penicillin 100 mg/mL streptomycin, and 50 μM 2-ME at 37°C with 5% CO_2 atmosphere. Cells were cultured in the presence of the different dendritic compound at the indicated concentrations.

Cell viability assay

The assay was performed by a variation of the method described by Mosmann.[29] Briefly, 8.0 x 10^3 MIN6 cells/well were cultured in 96 well plates. Concentrations that inhibited cell growth

by 50% (IC_{50}) after 72 h of treatment were calculated based on the survival rate compared with untreated cells. Relative cell viability was measured by the absorbance on an ELISA plate reader (Synergy, Bio-Tek, Winooski, VT, USA) at 550 nm.

Glucose-stimulated insulin secretion (GSIS) assay

Six replicates of groups of 8 islets were collected for each condition into 1.5 mL tubes and pre-incubated in Krebs-Ringer Bicarbonate buffer (KRB), containing 140 mM NaCl, 4.5 mM KCl, 2.5 mM $CaCl_2$, 1 mM $MgCl_2$, 20 mM HEPES, pH= 7.4, and supplemented with 0.1% BSA and 2.8 mM glucose for 30 min, followed by stimulation with 2.8 or 16.7 mM glucose for 1 h at 37 ºC. Supernatant was recovered and islets were lysed in 200 µL of acid-ethanol solution to measure insulin content. Insulin levels in supernatant and lysates were determined by insulin ELISA kit (Mercodia, Uppsala, Sweden), according to the manufacturer's protocol.

Statistical analysis

Data are presented as means ± SEM for at least three independent experiments in triplicate, as indicated in each experiment. Statistical significance between two groups was determined using Student's two-tailed t test, and differences among more than two groups were analysed by ANOVA. A p value <0.05 was accepted as significant (*).

Molecular modelling calculations

The dendrimers using in this work were built in three steps, the core of the dendrimer, internal dendrons, and terminal branches. All these components of dendrimer were parametrized separately, using CHARMM general force field and the force field toolkit of VMD.[30] The three different parts were combined to construct the dendrimers, following the descriptions of Marquez-Miranda et al.[31] After parametrization, the dendrimers were minimized and equilibrated using the NAMD v 2.1 software,[32] using 10000 step and 5ns of simulations, NPT ensemble at standard conditions (T=298 K and P=1 atm) solvated with TIP3P water model and neutralized with NaCl. The peptide Amiline (PDB: 2KB8) was download of the protein data bank and was build using the CHARMM36 protein force field.[33] The peptide was minimized and equilibrated using the same procedure for the dendrimers. After the energy minimization and equilibration, the more stable configuration of dendrimers and peptide was selected to build the final system. The systems of dendrimers and protein were built with a relation 1:1. The dendrimer was placed at a distance of 15 Å of the center of mass of protein, the system was solvated with a TIP3P water box and was neutralized with counterions NaCl. The molecular dynamics simulations were carried out with NAMD 2.1 software. All MD simulations were run under isobaric-isothermal NPT ensemble (T= 298 K, P= 1atm), with periodic boundary conditions and a TIP3P water box for 40 ns. To maintain constant pressure and temperature,

Langevin dynamics with a damping coefficient of 1 ps-1 and the Nose–Hoover Langevin piston method were applied. All hydrogen bonds were constrained during the MD simulations using the SHAKE algorithm. Long-range electrostatic interactions were calculated with the particle mesh Ewald algorithm, and Van der Waals forces were estimated using a cutoff of 10 Å. Equations of motion were integrated with a time step of 2 fs using the Verlet algorithm.

MM-GBSA (Molecular Mechanics-Generalized Born Surface Area) was used to estimate the binding free energy of the dendrimer−peptide complexes. The molecular structures were taken from the MD simulations of the complexes. For calculations, 20ns was extracted from a total of 40 ns production MD trajectories. The MM/GBSA analysis was performed on three subsets of each system: the peptide alone, the dendrimer alone, and the complex (dendrimer-peptide). The explicit TIP3P water molecules and ions were removed. The total free energy was calculated including all the molecular mechanics' contributions (bond, angle, and dihedral energies, electrostatic and van der Waals energies). The energetic contributions were calculated using NAMD 2.9 with the generalized Born implicit solvent model.

ASSOCIATED CONTENT

*Supporting Information: The Supporting Information is available free of charge on the ACS Publications website at DOI:

AUTHOR INFORMATION

Corresponding Authors*

E-mail: paula.ortega@uah.es

ORCID Paula Ortega López https://orcid.org/0000-0003-0377-5429

Notes: The authors declare no competing financial interest

ACKNOWLEDGMENTS

This work was supported by PIE14/00061 (CIBER), CTQ2017-86224-P (MINECO), Consortium IMMUNOTHERCAN-CM B2017/BMD-3733 (CAM), NANODENDMED II-CM ref B2017/BMD-3703 and project SBPLY/17/180501/000358 JCCM, Instituto de Salud Carlos III (PI14/00447), Fondecyt Regular projects 1170733 (F.G-N), the US Air Force Office of Scientific Research (AFOSR) under Award FA9550-16-1-0384 (Y.D, F.G-N) and the Centro Interdisciplinario de Neurociencia de Valparaiso is a Millennium Institute supported by the Millennium Scientific Initiative of the Chilean Ministry of Economy, Development, and Tourism (P029-022-F) (Y.D, F.G-N). CIBER-BBN is an initiative funded by the VI National R&D&i Plan 2008–2011, Iniciativa Ingenio 2010, Consolider Program, CIBER Actions and

financed by the Instituto de Salud Carlos III with assistance from the European Regional Development Fund.

REFERENCES

[1] M. Stefani, *Prog. Neurobiol.* **2012**, *99*, 226-245.

[2] V. E. Thomas, J. Smith, M. D. Benson, N. R. Dasgupta, *Neurodegener. Dis. Manag.* **2019**, *9*, 289-299.

[3] aD. Shea, C. C. Hsu, T. M. Bi, N. Paranjapye, M. C. Childers, J. Cochran, C. P. Tomberlin, L. B. Wang, D. Paris, J. Zonderman, G. Varani, C. D. Link, M. Mullan, V. Daggett, *Proceedings of the National Academy of Sciences of the United States of America* **2019**, *116*, 8895-8900; bP. Bourassa, C. Tremblay, J. A. Schneider, D. A. Bennett, F. Calon, *Acta Neuropathol.* **2019**, *137*, 801-823.

[4] aJ. Bu, J. S. Liu, K. Liu, Z. H. Wang, *Behav Brain Res* **2019**, *364*, 340-347; bA. Bougea, L. Stefanis, G. P. Paraskevas, E. Emmanouilidou, K. Vekrelis, E. Kapaki, *Neurol. Sci.* **2019**, *40*, 929-938; cI. van Steenoven, N. K. Majbour, N. N. Vaikath, H. W. Berendse, W. M. van der Flier, W. D. J. van de Berg, C. E. Teunissen, A. W. Lemstra, O. M. A. El-Agnaf, *Mov Disord* **2018**, *33*, 1724-1733.

[5] V. Banerjee, T. Shani, B. Katzman, M. Vyazmensky, N. Papo, A. Israelson, S. Engel, *ACS Chem. Neurosci* **2016**, *7*, 1595-1606.

[6] K. W. Drombosky, S. Rode, R. Kodali, T. C. Jacob, M. J. Palladino, R. Wetzel, *Neurobiol. Dis.* **2018**, *120*, 126-138.

[7] aE. Katorcha, N. Makarava, Y. J. Lee, I. Lindberg, M. J. Monteiro, G. G. Kovacs, I. V. Baskakov, *PLoS Pathog.* **2017**, *13*; bP. Piccardo, D. King, G. Telling, J. C. Manson, R. M. Barron, *J. Virol.* **2013**, *87*, 12349-12356.

[8] aF. Bellia, V. Lanza, S. Garcia-Vinuales, I. M. M. Ahmed, A. Pietropaolo, C. Iacobucci, G. Malgieri, G. D'Abrosca, R. Fattorusso, V. G. Nicoletti, D. Sbardella, G. R. Tundo, M. Coletta, L. Pirone, E. Pedone, D. Calcagno, G. Grasso, D. Milardi, *Chem. Sci.* **2019**, *10*, 2732-2742; bA. Tramutola, F. Triani, F. Di Domenico, E. Barone, J. Cai, J. B. Klein, M. Perluigi, D. A. Butterfield, *Neurobiol. Dis.* **2018**, *118*, 129-141.

[9] aA. Kanatsuka, S. Kou, H. Makino, *Diabetol. Int.* **2018**, *9*, 266-266; bS. Costes, *Curr. Opin. Pharmacol.* **2018**, *43*, 104-110; cV. Singh, N. Saluja, *NT J DIABETES DEV C.* **2016**, *36*, 477-489.

[10] aH. E. Cuevas, *ETHNIC HEALTH* **2019**, *24*, 512-526; bY. Lin, J. Wessel, *Curr Diab Rep* **2019**, *19*.

[11] L. Haataja, T. Gurlo, C. J. Huang, P. C. Butler, *Endoc. Rev.* **2008**, *29*, 303-316.

[12] S. Bose, J. Cho, *Ageing. Res. Rev.* **2017**, *35*, 155-175.

[13] aR. E. Carlisle, E. Brimble, K. E. Werner, G. L. Cruz, K. Ask, A. J. Ingram, J. G. Dickhout, *Plos One* **2014**, *9*; bS. Mimori, Y. Okuma, M. Kaneko, K. Kawada, T. Hosoi, K. Ozawa, Y. Nomura, H. Hamana, *Biol Pharm Bull* **2012**, *35*, 84-90.

[14] J. Montane, S. de Pablo, C. Castano, J. Rodriguez-Comas, L. Cadavez, M. Obach, M. Visa, G. Alcarraz-Vizan, M. Sanchez-Martinez, A. Nonell-Canals, M. Parrizas, J.-M. Servitja, A. Novials, *Faseb J.* **2017**, *31*, 5296-+.

[15] aT. G. Singh, S. Dhiman, *Nanocarriers as Nanomedicine: A Promising Platform for Drug Delivery in Nanopharmaceuticals*, **2016**; bN. Poovaiah, Z. Davoudi, H. Peng, B. Schlichtmann, S. Mallapragada, B. Narasimhan, Q. Wang, *Nanoscale* **2018**, *10*, 16962-16983.

[16] aY. Kim, E. J. Park, D. H. Na, *Arch. Pharmacal Res* **2018**, *41*, 571-582; bH. J. Hsu, J. Bugno, S. R. Lee, S. Hong, *Wiley Interdiscip Rev Nanomed Nanobiotechnol.* **2017**, *9*.

[17] G. Sekar, I. Florance, A. Sivakumar, A. Mukherjee, N. Chandrasekaran, *Int. J. Biol. Macromol.* **2016**, *93*, 1007-1018.

[18] aA. Janaszewska, B. Klajnert-Maculewicz, M. Marcinkowska, P. Duchnowicz, D. Appelhans, G. Grasso, M. A. Deriu, A. Danani, M. Cangiotti, M. F. Ottaviani, *Nano Res.*

2018, *11*, 1204-1226; bM. F. Ottaviani, M. Cangiotti, L. Fiorani, A. Fattori, T. Wasiak, D. Appelhans, B. Klajnert, *Curr Med Chem* **2012**, *19*, 5907-5921.
[19] T. Wasiak, M. Marcinkowska, I. Pieszynski, M. Zablocka, A. M. Caminade, J. P. Majoral, B. Klajnert-Maculewicz, *New J. Chem.* **2015**, *39*, 4852-4859.
[20] K. Milowska, A. Szwed, M. Mutrynowska, R. Gomez-Ramirez, F. J. de la Mata, T. Gabryelak, M. Bryszewska, *Int. J. Pharma.* **2015**, *484*, 268-275.
[21] E. N. Gurzov, B. Wang, E. H. Pilkington, P. Y. Chen, A. Kakinen, W. J. Stanley, S. A. Litwak, E. G. Hanssen, T. P. Davis, F. Ding, P. C. Ke, *Small* **2016**, *12*, 1615-1626.
[22] O. Klementieva, N. Benseny-Cases, A. Gella, D. Appelhans, B. Voit, J. Cladera, *Biomacromolecules* **2011**, *12*, 3903-3909.
[23] P. T. Nguyen, R. Sharma, R. Rej, C. A. De Carufel, R. Roy, S. Bourgault, *Rsc Adv.* **2016**, *6*, 76360-76369.
[24] E. Fuentes-Paniagua, J. Sanchez-Nieves, J. M. Hernandez-Ros, A. Fernandez-Ezequiel, J. Soliveri, J. L. Copa-Patino, R. Gomez, F. Javier de la Mata, *Rsc Adv.* **2016**, *6*, 7022-7033.
[25] E. Fuentes-Paniagua, J. M. Hernández-Ros, M. Sánchez-Milla, M. A. Camero, M. Maly, J. Pérez-Serrano, J. L. Copa-Patiño, J. Sánchez-Nieves, J. Soliveri, R. Gómez, F. Javier de la Mata, *Rsc Adv.* **2014**, *4*, 1256-1265.
[26] M. Henson, B. Buman, K. Jordan, E. Rahrmann, R. Hardy, K. Johnson, T. O'Brien, *Amyloid* **2007**, *13*, 250-259.
[27] K. Pillay, P. Govender, *BioMed. Res. Int.* **2013**, *2013*, 17.
[28] A. J. Perisé-Barrios, E. Fuentes-Paniagua, J. Sánchez-Nieves, M. J. Serramía, E. Alonso, R. M. Reguera, R. Gómez, F. J. de la Mata, M. Á. Muñoz-Fernández, *Mol. Pharma.* **2016**, *13*, 3427-3438.
[29] aT. Mosmann, *J. Immunol. Methods* **1983**, *65*, 55-63; bG. Alcarraz-Vizán, J. Boren, W.-N. P. Lee, M. Cascante, *Metabolomics* **2010**, *6*, 229-237.
[30] C. G. Mayne, J. Saam, K. Schulten, E. Tajkhorshid, J. C. Gumbart, *J. Comput. Chem.* **2013**, *34*, 2757-2770.
[31] V. Marquez-Miranda, J. Abrigo, J. C. Rivera, I. Araya-Duran, J. Aravena, F. Simon, N. Pacheco, F. D. Gonzalez-Nilo, C. Cabello-Verrugio, *Int J. Nanomed.* **2017**, *12*, 1985-1999.
[32] J. C. Phillips, R. Braun, W. Wang, J. Gumbart, E. Tajkhorshid, E. Villa, C. Chipot, R. D. Skeel, L. Kale, K. Schulten, *J. Comput. Chem.* **2005**, *26*, 1781-1802.
[33] J. Huang, A. D. MacKerell, *J. Comput. Chem.* **2013**, *34*, 2135-2145.